لجمـــهوريـــة الـجـــزائرِيـــة الدِيـمقراطـيـــــــة الشـعـبـيـــــة
THE PEOPLE'S DEMOCRATIC REPUBLIC OF ALGERIA
وزارة الدعـلـيـم الـعـالـــي والـبـحـث الـعـلـمي
THE MINISTRY OF HIGHER EDUCATION AND SCIENTIFIC RESEARCH
جـامـعـة عـمارثـلـيـــجـــي بألاغـــواط
AMAR TELIDJI UNIVERSITY OF LAGHOUAT

كـلـيـــة الـتـكـنـولـوجـيا
FACULTY OF TECHNOLOGY
قسم االلكتروتـقـنـي
DEPARTMENT OF ELECTROTECHNIC

Master's dissertation

Domain : Sciences and Technologies
Field : Automatic
Option : Automatic and system

Theme

Neural control by DTC of a permanent magnet synchronous motor powered by a photovoltaic generator

Presented by :
Mr : Far Abouelkacem
Mr : Chikhaoui Yacine

Publicly supported ahead of a jury composed of :

Mr : Benmouiza Khalil	Professor	Chairman
Mr : Bessedik Sid ahmed	Professor	Examiner
Mss : katia Kouzi	Professor	Examiner
Mr : Ameur Aissa	Professor	Supervisor
Mr : Benmilod Ismail	Prof	Co-Supervisor

Academic year 2022/2023

Acknowledgments

As we approach graduation, we find ourselves thinking about the amazing journey that has led us to this moment. Along this path, there have been countless individuals who have played an important role in shaping academic and personal growth. We wanted to take a moment to express our deep gratitude for your support and guidance during my educational endeavors.

First and foremost, we would like to express our sincere appreciation to the family.

At the end of this work, we would like to thank our supervisor **Mr.Amer aissa** and **Mr.Ismail ben miloud** for his support, guidance and constructive criticism. And to our professors and teachers **Mr.Benmouiza khlil** and **Mr Oubbati youcef**, we are so profoundly grateful for the knowledge and wisdom you have imparted to us.

We would also like to thank our friends and classmates. The friendships and camaraderie we shared made our learning journey even more enriching and unforgettable.

We thank you, from the bottom of our hearts, for being a part of our journey and for contributing to our growth and success. Your impact on our lives will forever be appreciated, and we hope to make you proud as we seize the opportunities that lie ahead.

With sincere gratitude

الملخص:

تركز هذه الدراسة على التحكم العصبي عن طريق التحكم المباشر في عزم الدوران لمحرك متزامن ذو مغناطيس دائم مدعوم بمولد كهروضوئي. تم تصميم المحرك وتحديد خصائصه، ثم تم استكشاف التحكم المباشر في عزم الدوران وفعاليته. وتضمنت الخطوة التالية فهم مصدر الطاقة للمحرك، وهو المولد الكهروضوئي، بما في ذلك خصائصه وتأثير درجة الحرارة والإضاءة على النظام. وأخيرا، قدمنا لمحة عامة عن العنصر الأخير في نظام التحكم، وهو التحكم العصبي.

الكلمات المفتاحية:

المحرك المتزامن ذو المغنطيس الدائمة , التحكم المباشر في عزم الدوران ,الكهروضوئي ,الشبكات العصبية الاصطناعية .

Abstract:

This study focuses on the investigation of neural control by direct torque control of a permanent magnet synchronous motor powered by a photovoltaic generator . The motor was modeled and its characteristics were identified, followed by an exploration of direct torque control and its effectiveness. The next step involved understanding the power source for the motor, which is the photovoltaic generator, including its characteristics and the impact of temperature and illumination on the system. Finally, we provided an overview of the last component of the control system, which is neural control.

Keywords:

Permanent Magnet Synchronous Motor (PMSM), Direct Torque Control (DTC), Photovoltaic (PV), Artificial neural networks (ANN)

Résumé:

Cette étude porte sur l'étude du contrôle neuronal par contrôle direct du couple d'un moteur synchrone à aimants permanents alimenté par un générateur photovoltaïque. Le moteur a été modélisé et ses caractéristiques ont été identifiées, suivi d'une exploration du contrôle direct du couple et de son efficacité. L'étape suivante consistait à comprendre la source d'alimentation du moteur, qui est le générateur photovoltaïque, y compris ses caractéristiques et l'impact de la température et de l'éclairage sur le système. Enfin, nous avons donné un aperçu du dernier composant du système de contrôle, qui est le contrôle neuronal.

Mots clés :

Moteur Synchrone à Aimants Permanents (MSAP), Contrôle Direct de Couple (DTC), Photovoltaïque (PV), Réseaux de neurones artificiels (RNA).

Acronyms

Abridged Words

PMSM : Permanent Magnet Synchronous Motor.

EMF : Electromotive force.

AF : Increase flux.

AC : increase the torque.

DF : Decrease flux.

DC : Decrease the torque.

$E.M.F$: Electromotive force.

$IGBT$: Insulated-gate bipolar transistor.

DTC : Direct torque control.

FOC : Field-of-control.

IPM :Internal permanent magnet.

PWM : Pulse-width modulation.

PV : Photovoltaic

$MPPT$: Maximum power point tracking.

$L3P$: Lumped, 1 Mechanism model with 3 Parameters

Model Parameters

V_s : stator voltage vector

i_s : stator current vector

ϕ_s : stator flux vector

R_s : Resistance of a stator phase

θ : electrical angle between the a axis and the d axis

ω_r : rotational speed of the rotating field

Ω_r : mechanical rotational speed of the rotor

p : number of pole pairs

C_em : the electromagnetic torque

C_r : resistive torque

f_r : the friction coefficient

J : is the moment of inertia

a, b, c : Variables expressed in the three-phase fixed benchmark

$d.q$: Variables expressed in the fixed frame (d,q) rotating at synchronous speed

$\alpha.\beta$: Variables expressed in the two-phase fixed frame (α,β)

$\bar{\phi_s}$: is the stator flux vector

$\bar{\phi_{s'}}$: is the rotor flux vector brought back to the stator

δ : is the angle between the stator and rotor flux vectors

C_e^* : The torque setpoint

I_{ph} : photonic current

I_{d1} : diode current 1

I_{d2} : diode current 2

$V_t = KT_c/q$: representing the thermodynamic potential

T_c : is the absolute temperature

q : electron charge constant,

I_{sh} : Current flows through the shunt resistor

E : illumination

T : temperature in

I_{ph0} : photo-current generated by the diode

E_g : Gap energy of the semiconductor

.

Contents

Bibliography

List of Tables

List of Figures

General Introduction

1. Problem Formulation

Today, permanent magnet synchronous motors (PMSM) are highly recommended in the industrial sector. This is due to their simplicity, reliability, and compactness compared to DC motors. As a result, their construction is more straightforward as they do not require mechanical switches. This simplicity contributes to their longer lifespan and eliminates the need for regular maintenance. Another advantage is their suitability for use in explosive environments since they do not produce sparks. Additionally, PMS motors offer significant power output relative to their mass, unlike DC machines that require multiple power sources and have lower power density.[4]

In this Dissertation , the focus is on defining the problem statement and setting the objectives of the study. The aim is to investigate the feasibility and effectiveness of utilizing neural control algorithms in the DTC scheme for a PMSM powered by a photovoltaic (PV) generator. The challenges and limitations associated with conventional control methods will be addressed, highlighting the potential benefits of neural control approaches.

2. Dissertation Outline

The dissertation will follow a structured framework to achieve the research objectives. The outline will cover the following key aspects:

The first chapter: The mathematical modeling of the PMSM system and the DC-AC converter will be studied, and at the end of the chapter, a simulation of the motor.

The second chapter: we will know the direct control of torque and then present a general diagram of the stages of this control, after that we will learn about the stages of direct control of torque in detail and all the mathematical equations that are effective in this control.finally, the results of the motor with direct torque control are simulated.

The third chapter:,The chapter will present the photovoltaic systems, which we consider as the source of power for the engine.

In the last chapter we will discuss the role of neural networks in motor control, specifically in direct torque control.and we will learn about the natural effects on them. We will also present the integration of the above topics, including the solar energy system as the energy source and the control of neural networks in direct torque control of the motor.

Conclusion and Future Work: The thesis will conclude with a summary of the findings, key contributions, and recommendations for further research in the field of neural control for PMSMs powered by photovoltaic systems.

Chapter I

Generality and modelling of PMSM

I.1 Introduction

A synchronous motor, as the name suggests, runs under steady-state conditions at a fixed speed called the synchronous speed. The synchronous speed, depends only upon the frequency of the applied voltage and the number of poles in the machine. In other words, the speed of a synchronous motor is independent of the load as long as the load is within the capability of the motor. If the load torque exceeds the maximum torque that can be developed by the motor, the motor simply comes to rest and the average torque developed by it is zero. For this reason, a synchronous motor is not inherently self-starting. Therefore, it must be brought up almost to its synchronous speed by some auxiliary means before it can be synchronized to the supply .[16]

Permanent Magnet Synchronous Motors (PMSM) are widely used in high-performance drives such as industrial robots, automotive hybrid drive trains and machine tools thanks to their advantages as: high efficiency, high power density, high torque/inertia ratio, and free maintenance. In the recent years, the magnetic and thermal capabilities of the Permanent Magnet (PM) have been considerably increased by employing the high-coercive permanent magnet material.[11]

A synchronous motor can be either a single-phase or a polyphase motor. Only three-phase synchronous motors are discussed in this chapter, but the development is valid for any polyphase synchronous motor[16].

I.2 Permanent magnet Synchronous motor(PMSM)

Researchers have made numerous attempts to produce synchronous motors with magnets. However, it was only after the introduction of materials with a strong coercive field and fairly high remnant induction that they were able to successfully materialize. In permanent magnet synchronous machines, the magnets are located on the rotating part while the stator consists of a sinusoidally distributed three-phase winding. The operation of these machines is based on the principle of the magnetic field rotating in synchronism with the rotor, hence the name permanent magnet synchronous machines (PMSM). In most applications, an inverter is required to provide a power supply with variable voltage and frequency.[8].

I.3 Structure of PMSM

The synchronous motor is composed of two parts, a moving part or rotor and a fixed part or stator that carries windings. The space between these two elements is known as the air gap.

Figure I.1: Structure of permanent magnet synchronous motor.[1]

I.3.1 The Stator

The stator of a synchronous motor is similar to that of an asynchronous motor, as it has a three-phase winding formed by identical windings displaced from each other by 120. The windings can be either star-coupled (which cancels the unipolar current component) or triangular-shaped, distributed in notches and carried in a laminated magnetic circuit. This winding constitutes the armature of the machine, as it is where electromotive forces are induced by the rotating field created by the rotor.[17]

I.3.2 The Rotor

A rotor in a permanent magnet synchronous motor (PMSM) is a rotating component that contains permanent magnets, The magnetic field produced by the permanent magnets interacts with the stator's magnetic field, which is created by the stator windings, to produce torque that drives the motor's rotation. In PMSM, the rotor rotates synchronously with the rotating magnetic field generated by the stator, which is why they are called "synchronous" motors.[17]

I.4 Starting PMSM

A synchronous motor won't start by itself because it requires a rotating magnetic field to be present in order to synchronize its own magnetic field and start rotating at a constant speed. Unlike an induction motor, which can start on its own due to the rotating magnetic field created by the AC power supply.

there are three basic approaches that be used to safely start a synchronous motor:

I.4.1 Variable frequency drive

To start a synchronous motor, the stator magnetic fields must rotate at a low enough speed for the rotor to lock in, and then the speed can be gradually increased to operating speed. However, the problem is where to get the variable electrical frequency from, as regular power systems are regulated at 50 or 60 Hz. Solid-state motor controllers can convert a constant input frequency to any desired output frequency, making it possible to control the electrical frequency applied to the motor. With a variable-frequency drive unit included in the motor-control circuit, the synchronous motor can be started by adjusting the frequency to a low value and then increasing it to the desired operating frequency. The voltage in any variable-frequency drive or variable-frequency starter circuit must vary roughly linearly with the applied frequency[3][2].

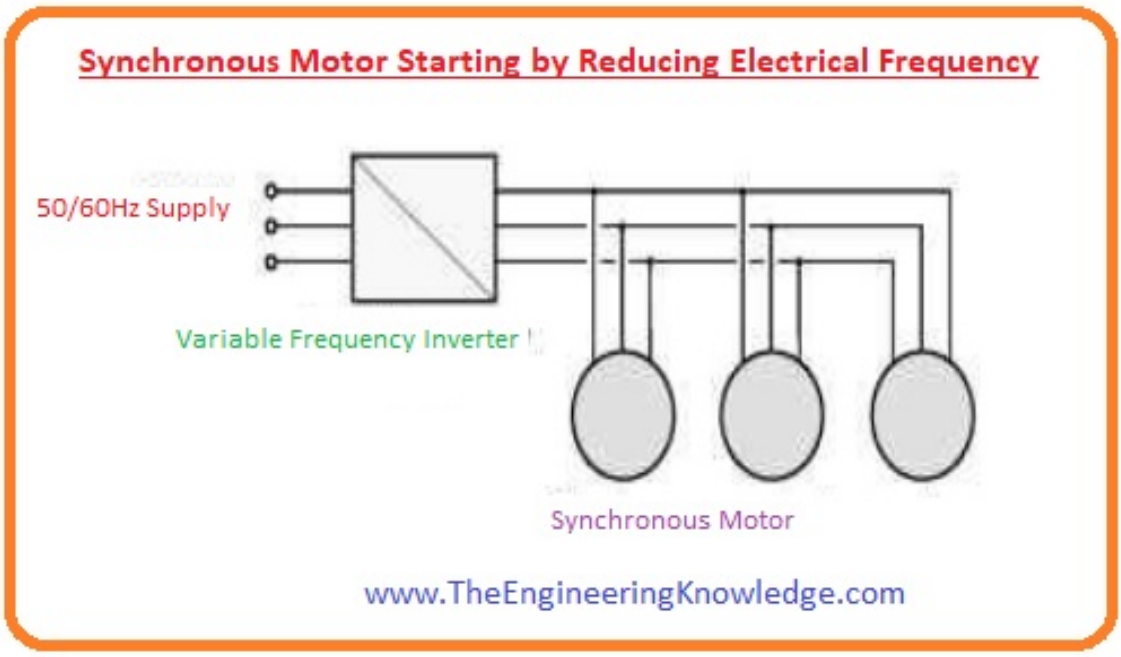

Figure I.2: variable frequency inverter

I.4.2 External mover

To start a synchronous motor, an external starting motor can be attached to bring it up to full speed, then it can be paralleled with its power system as a generator and the starting motor can be detached. This procedure is common in motor-generator sets and the starting motor only needs to overcome the motor's inertia. It's possible to use brushless excitation systems mounted on the shafts of synchronous motors as starting motors. For some synchronous motors, an external starting motor or using the exciter may be the only option due to the power system's inability to handle the starting currents needed for other approaches.[2][3]

Figure I.3: External mover[2]

.

I.4.3 Amortisseur Windings

Starting a synchronous motor with the help of amortisseur windings refers to a method of starting a synchronous motor by using a secondary set of windings that are embedded in the motor's rotor. These windings are also known as damper or squirrel cage windings.

When a synchronous motor is started, the stator winding is energized to create a magnetic field. However, the rotor of the motor does not rotate synchronously with the magnetic field, as it is not yet energized. This can cause the motor to stall or jerk.

To prevent this, the amortisseur windings are used. These windings create a magnetic field that is slightly out of phase with the magnetic field of the stator winding. As a result, the rotor starts to rotate, and the motor gradually synchronizes with the stator magnetic field.[3]

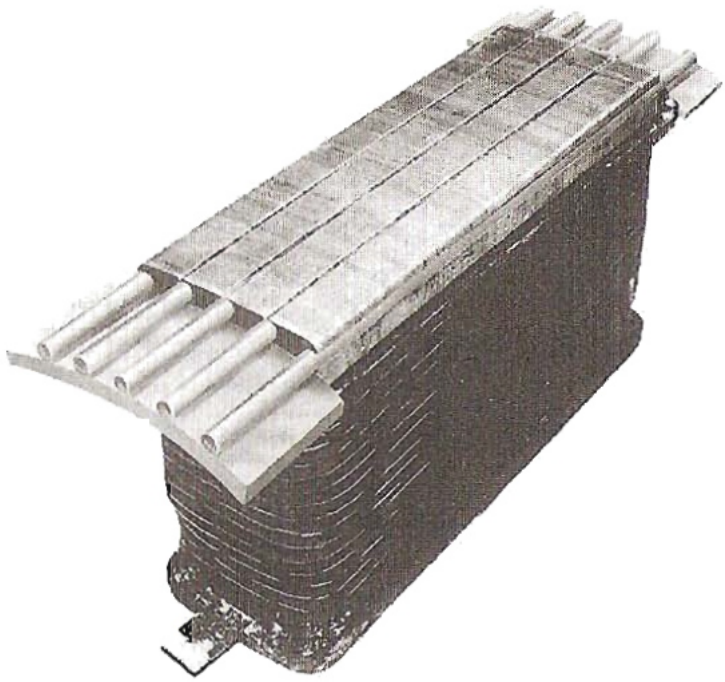

Figure I.4: Amortisseur Windings.[3]

Once the motor reaches synchronous speed, the amortisseur windings are no longer needed and become inactive. The motor continues to operate at synchronous speed by locking in with the rotating magnetic field of the stator winding[3].

Overall, using amortisseur windings to start a synchronous motor provides a reliable and efficient way to bring the motor up to speed without the risk of stalling or damage.

I.5 Advantages and disadvantages of PMSM

I.5.1 advantages

- High efficiency: PMSM have a high efficiency compared to other types of electric motors,This makes them ideal for applications where energy efficiency is important, such as electric vehicles, industrial equipment, and home appliances.
- High power density: PMSM have a high power density, which means they can produce a lot of power in a small size. This makes them ideal for applications where space is limited, such as in electric vehicles and drones.
- High torque density: PMSM have a high torque density, which means they can produce a lot of torque in a small size. This makes them ideal for applications where high torque is required, such as in robotics and industrial equipment.

- Low maintenance: PMSM have a simple design with fewer moving parts, which means they require less maintenance compared to other types of electric motors. This results in reduced downtime and lower maintenance costs.
- Precise control: PMSM can be easily controlled using modern electronics, which allows for precise control of speed and torque. This makes them ideal for applications where precise control is required, such as in robotics and machine tools.
- Durability: PMSM have a long life span due to their simple design and the use of permanent magnets, which are not subject to wear and tear. This results in a lower total cost of ownership over the life of the motor.
- Overall, the benefits of PMSM make them an attractive choice for a wide range of applications, including electric vehicles, industrial equipment, robotics, and home appliances[18][8].

I.5.2 disadvantages

- Cost: PMSMs can be more expensive than other types of electric motors, due to the cost of the permanent magnets used in their construction. However, the cost has been decreasing as the technology has improved.
- Temperature sensitivity: PMSM can be sensitive to temperature changes, especially at high temperatures. This can lead to a decrease in performance or even damage to the motor. Proper cooling and thermal management systems are required to ensure reliable operation.
- Control complexity: While PMSM are easily controlled using modern electronics, the control systems can be complex and require advanced knowledge and expertise to design and implement. This can be a challenge for some manufacturers and end-users.
- Limited availability: Permanent magnets used in PMSM are made from rare-earth materials, which can be expensive and have limited availability. This can be a concern in some industries, especially as demand for PMSM increases.
- Overall, the disadvantages of PMSM are relatively minor compared to their many advantages, and advancements in technology are continuously addressing these issues[8].

I.6 Modelling of PMSM

The study of any physical system requires modelling, it allows us to simulate the behavior of this system in the face of different operating conditions and thus understand the mechanisms governing its operation, the modelling of the PMSM is the subject of many studies on medium

and high power. The form of a mathematical model of an PMSM largely facilitates its study.[4][8]

The physical phenomena inherent in the functioning of the system can be partially or completely taken into account in a model. They result in several levels of modelling linked to associated simplifying hypotheses. These simplifications come from the properties of alternative current machines. For this purpose, the following assumptions are adopted:[4][8]

- The magnetic circuit of the machine and not saturated
- Sinusoidal distribution of the E.M.F
- The effect of the temperature on the resistors is negligible
- hysteresis and eddy currents are negligible
- The skin effect that increases resistances and reduces inductances is negligible
- the air gap is of uniform thickness
- The notch effect is not taken into account

I.7 Equations of the model of PMSM

The figure (I.5) gives the representation of stator windings and the flux of rotor magnets for a three -phase synchronous motor with permanent magnets

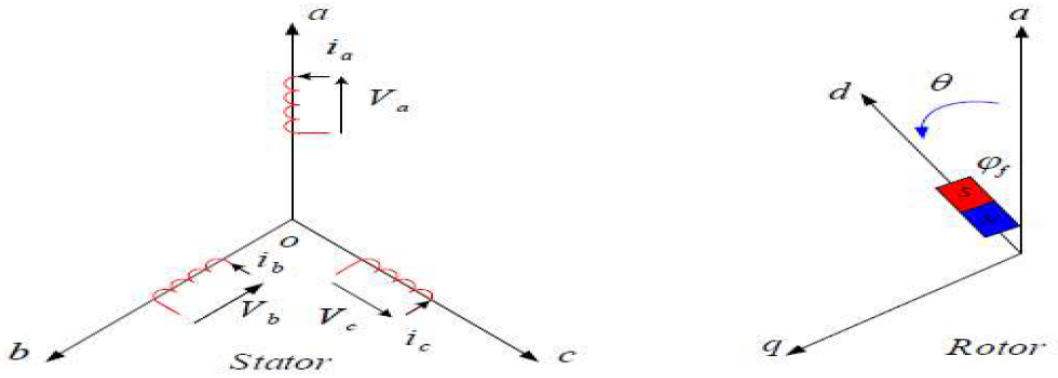

Figure I.5: Schematic representation of the windings of the PMSM[4]

The mathematical model of the PMSM is similar to that of the classic synchronous machine, within the framework of the simplifying hypotheses announced previously and for a symmetrical machine, the electrical, magnetic and mechanical equations are written as follows:

I.7.1 Electric equations

$$[V_s(t)] = R_s[i_s(t)] + \frac{d[\phi_s(t)]}{dt} \tag{I.1}$$

with:

$[V_s(t)] = [V_a(t)V_b(t)V_c(t)]^t$: stator voltage vector;

$[i_s(t)] = [i_a(t)i_b(t)i_c(t)]^t$: stator current vector;

$[\phi_s] = [\phi_a\phi_b\phi_c]^t$: stator flux vector;

R_s: Resistance of a stator phase.

or:

$$\begin{cases} V_a(t) = R_s i_a(t) + \frac{d\phi_a(t)}{dt} \\ V_b(t) = R_s i_b(t) + \frac{d\phi_b(t)}{dt} \\ V_c(t) = R_s i_c(t) + \frac{d\phi_c(t)}{dt} \end{cases} \tag{I.2}$$

I.7.2 Magnetic equations

$$[\phi_s(t)] = [L_s][i_s(t)] + [\phi_r(t)] \tag{I.3}$$

with:

$[L_s] = \begin{bmatrix} L_a & M_{ab} & M_{ac} \\ M_{ab} & L_b & M_{bc} \\ M_{ac} & M_{bc} & L_c \end{bmatrix}$: stator inductance matrix.

or:

$$\begin{cases} \phi_a(t) = L_a i_a(t) + M_{ab} i_b(t) + M_{ac} i_c(t) + \phi_{rm}\cos(\theta) \\ \phi_b(t) = L_b i_b(t) + M_{ab} i_a(t) + M_{bc} i_c(t) + \phi_{rm}\cos(\theta - \frac{2\pi}{3}) \\ \phi_c(t) = L_c i_c(t) + M_{ac} i_c(t) + M_{bc} i_b(t) + \phi_{rm}\cos(\theta - \frac{4\pi}{3}) \end{cases} \tag{I.4}$$

or

$[\phi_r(t)]$ is the vector of the fluxes generated by the magnets in the rotor phases such that:

$$[\phi_r(t)] = \phi_{rm}[\cos(\theta) \quad \cos(\theta - \frac{2\pi}{3}) \quad \cos(\theta - \frac{4\pi}{3})]^t \tag{I.5}$$

and :

ϕ_{rm} is the peak value of the flux created by the magnets

we have :

$$\theta = \int_0^t \omega_r(t)dt \tag{I.6}$$

$$\omega_r(t) = p\Omega_r(t) \tag{I.7}$$

with :

θ : electrical angle between the a axis and the d axis;

ω_r : rotational speed of the rotating field;

Ω_r : mechanical rotational speed of the rotor;

p : number of pole pairs;

I.7.3 Mechanical equations

$$J\frac{d\Omega_r(t)}{dt} = C_{em} - C_r - f_r\Omega_r(t) \tag{I.8}$$

Or :

C_{em} : is the electromagnetic torque.

C_r : is resistive torque.

f_r : is the friction coefficient.

J : is the moment of inertia.

furthermore the electromagnetic torque is expressed by :

$$C_{em} = [i_s(t)]^t[\frac{1}{2}\frac{d([L_s][i_s(t)])}{d\theta} + \frac{1}{2}\frac{d[\phi_r(t)]}{d\theta}] \tag{I.9}$$

I.8 Transformation of three-phase to two-phase

The Park transformation consists of a three-phase to two-phase transformation, followed by a rotation. It enables the conversion from the reference a,b,c frame to the α, β frame, and then to the d,q frame. The α, β frame remains fixed relative to the a,b,c frame, while the d,q frame is

movable. It forms an angle, known as the Park transformation angle or Park angle, with the fixed α, β reference.

I.8.1 Clarke's transform

The transition from a three-phase system (a,b,c) to a Clarke two-phase system (α,β) write:

$$\begin{bmatrix} X_\alpha \\ X_\beta \end{bmatrix} = \frac{2}{3} \begin{bmatrix} 1 & -\frac{1}{2} & -\frac{1}{2} \\ 0 & \frac{\sqrt{3}}{2} & -\frac{\sqrt{3}}{2} \end{bmatrix} \begin{bmatrix} X_a \\ X_b \\ X_c \end{bmatrix} \tag{I.10}$$

The inverse passage is write:

$$\begin{bmatrix} X_a \\ X_b \\ X_c \end{bmatrix} = \frac{2}{3} \begin{bmatrix} 1 & 0 \\ -\frac{1}{2} & \frac{\sqrt{3}}{2} \\ -\frac{1}{2} & -\frac{\sqrt{3}}{2} \end{bmatrix} \begin{bmatrix} X_\alpha \\ X_\beta \end{bmatrix} \tag{I.11}$$

The choice of the non normed passage matrix (Clarke) is practical in order where one deals with quantities d, q. This allows, for example, to directly assess the modulus of the current absorbed by the motor.

I.8.2 Park's basic transformation

The Park transformation makes it quite easy to deal with all the transient regimes of the poly-phase electric machine. The principle consists of replacing the quantities (current, voltage and flux) with real indices a, b, c by quantities with indices d, q, o (direct, in quadrature and homopolar) using the matrix of Park $[P(\theta)]$.

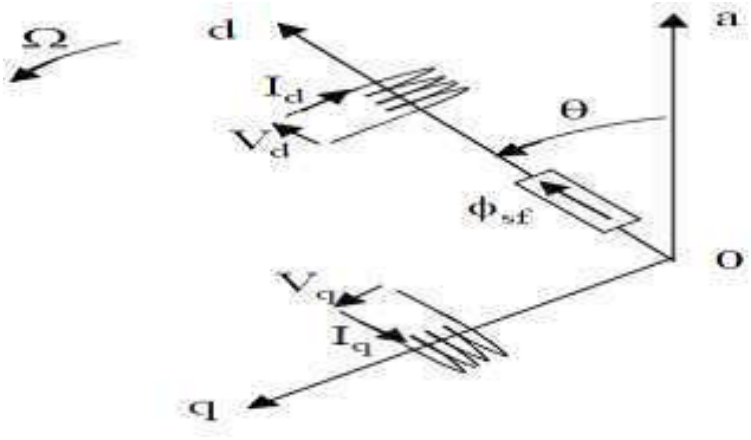

Figure I.6: Equivalent diagram of the motor in the reference (d, q)[5].

$$\begin{bmatrix} X_d \\ X_q \\ X_o \end{bmatrix} = [P(\theta)] \begin{bmatrix} X_a \\ X_b \\ X_c \end{bmatrix} \tag{I.12}$$

$$[P(\theta)] = \frac{2}{3} \begin{bmatrix} \cos(\theta) & \cos(\theta - \frac{2\pi}{3}) & \cos(\theta - \frac{2\pi}{3}) \\ -\sin(\theta) & -\sin(\theta - \frac{4\pi}{3}) & -\sin(\theta - \frac{4\pi}{3}) \\ \frac{1}{2} & \frac{1}{2} & \frac{1}{2} \end{bmatrix} \tag{I.13}$$

Whereas when we want to obtain X_d, X_q, X_0:

$$\begin{bmatrix} X_a \\ X_b \\ X_c \end{bmatrix} = [P(\theta)]^{-1} \begin{bmatrix} X_d \\ X_q \\ X_o \end{bmatrix} \tag{I.14}$$

And its inverse has the expression:

$$[P(\theta)]^{-1} = \begin{bmatrix} \cos(\theta) & -\sin(\theta) & 1 \\ \cos(\theta - \frac{2\pi}{3}) & -\sin(\theta - \frac{2\pi}{3}) & 1 \\ \cos(\theta - \frac{4\pi}{3}) & -\sin(\theta - \frac{4\pi}{3}) & 1 \end{bmatrix} \tag{I.15}$$

$[P(\theta)]$: Park's direct passage matrix

The motor is supposed to be symmetrical and connected in star, it therefore absorbs a balanced system of currents ($i_a + i_b + i_c = 0$).

I.8.3 Park transformation application on PMSM

Choosing a Park frame (d,q) related to the rotor and applying the transformation (I.12) to the system of electrical equations (I.1), we obtain:

$$[V_{dq0}(t)] = [P](\theta)[V_{abc}(t)] = R_s[P(\theta)][i_{abc}(t)] + [P(\theta)]\frac{d}{dt}[\phi_{abc}(t)] \tag{I.16}$$

then, basing on (I.12) and (I.1) we get :

$$[V_{dqo}(t)] = R_s[I_{dqo}(t)] + [P(\theta)][P(\theta)]^{-1}\frac{d}{dt}[\phi_{dqo}(t)] + [P(\theta)](\frac{d}{dt}[P(\theta)]^{-1})[\phi_{dqo}(t)] \tag{I.17}$$

After simplification, one can deduce Park's equations in vector form as :

$$[V_{dq}(t)] = R_s[I_{dq}(t)] + \frac{d}{dt}[\phi_{dq}(t)] + \omega_r[\phi^*_{dq}(t)] \tag{I.18}$$

or :

$$[V_{dq}] = \begin{bmatrix} V_d \\ V_q \end{bmatrix}, [i_{dq}] = \begin{bmatrix} I_d \\ I_q \end{bmatrix}, [\phi_{dq}] = \begin{bmatrix} \phi_d \\ \phi q \end{bmatrix}, [\phi^*_{dq}] = \begin{bmatrix} -\phi_q \\ \phi_d, \end{bmatrix}$$

furthermore the transformation (I.10) applied to the magnetic equations (I.3) gives :

$$\begin{bmatrix} \phi_d \\ \phi q \end{bmatrix} = \begin{bmatrix} Ld & 0 \\ 0 & Lq \end{bmatrix} \begin{bmatrix} Id \\ Iq \end{bmatrix} + \begin{bmatrix} \phi_{rm} \\ 0 \end{bmatrix} \tag{I.19}$$

The electromagnetic torque is produced by the interaction between the poles formed by the rotor magnets and the poles generated by the FMMs in the air gap generated by the stator currents. This torque developed by emf permanent magnet synchronous motor. sinusoidal and without damper can be expressed in Park's frame by:

$$C_{em} = \frac{3}{2}p[(L_d - L_q)I_d I_q + \phi_{rm} I_q] \tag{I.20}$$

In the case where the motor has smooth poles (La La), this equation is simplified as follows:

$$C_{em} = \frac{3}{2}p\phi_{rm} i_q \tag{I.21}$$

I.9 Modeling of the three-phase MLI voltage inverter

A voltage inverter is a static converter that provides DC-AC conversion. It is typically powered by a DC voltage source. The maximum power transmitted is determined by the specific characteristics of the receiver, in this case, the permanent magnet synchronous motor. There are several voltage inverter structures, each adapted to a specific application or specification. In our study, we focus on a classic MLL three-phase voltage inverter. It consists of three arms that use two switches, which are bidirectional in current and controlled for priming and blocking. The switches can be made using MOS transistors, IGBT, or GTO, depending on the desired power control and switching frequency. These switches are associated with antiparallel diodes to achieve current reversibility.[[19]].

I.10 Equation of the three-phase voltage inverter

We consider that the stator of the synchronous machine is star-connected. The inverter output voltages (V_{ao}, V_{bo}, V_{co}), are referenced with respect to a midpoint of a fictitious input 0 divider bridge. The neutral of the machine is not connected to the midpoint 0 of the inverter. therefore the sum of the currents of the stator phases is zero. In this case, the measurement of two phase currents is sufficient. Figure (I.7) illustrates the structure of this three-phase inverter.[20][6]

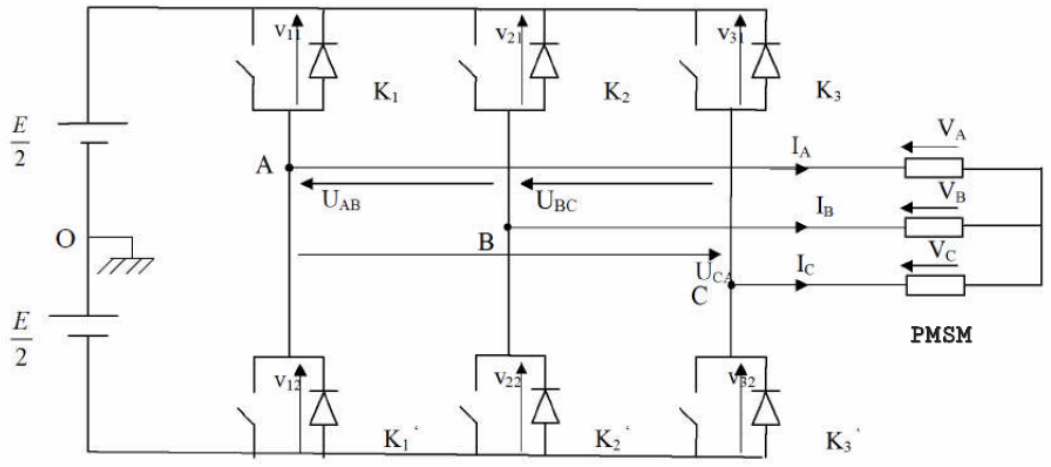

Figure I.7: diagram of a three-phase voltage inverter supplying the stator of the motor.[6]

We have K_i and $K_i^{'}$ (with i = 1,2,3): are the switches of the inverter and C_i is the control signals of the arms K of the inverter; with.

define a state function E_i' of its switches such that:

$$\begin{cases} C_i = 1 \;\; if \;\; K_i \; is \; closed \; K_i^{'} \; is \; open. \\ C_i = 0 \;\; if \;\; K_i \; is \; open \; K_i^{'} \; is \; closed. \end{cases}$$

The following figure (Fig.I.8) makes the link between the different switching sequences, the voltage vectors and the state of the switches forming the inverter.

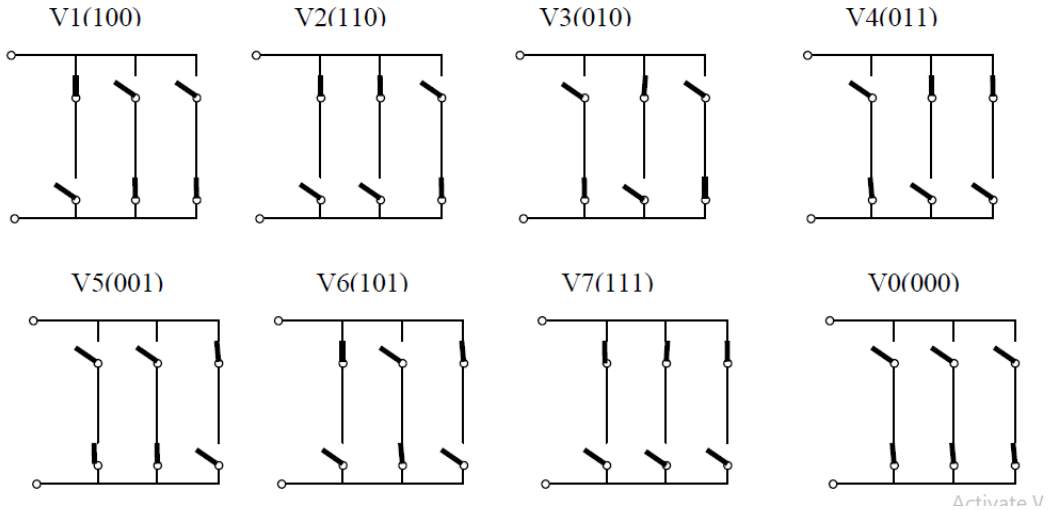

Figure I.8: State of switches for each voltage vector.[7]

we also have :

$$\begin{cases} V_a(t) = V_{an}(t) = V_{ao}(t) + V_{on}(t) \\ V_b(t) = V_{bn}(t) = V_{bo}(t) + V_{on}(t) \\ V_c(t) = V_{cn}(t) = V_{co}(t) + V_{on}(t) \end{cases} \tag{I.23}$$

with :

$$V_a(t) = V_b(t) = V_c(t) = 0 \tag{I.24}$$

What gives :

$$\begin{bmatrix} V_a(t) \\ V_b(t) \\ V_c(t) \end{bmatrix} = \frac{1}{3} \begin{bmatrix} 2 & -1 & -1 \\ -1 & 2 & -1 \\ -1 & -1 & 2 \end{bmatrix} \begin{bmatrix} V_{ao}(t) \\ V_{bo}(t) \\ V_{co}(t) \end{bmatrix} = \frac{E}{6} \begin{bmatrix} 2 & -1 & -1 \\ -1 & 2 & -1 \\ -1 & -1 & 2 \end{bmatrix} \begin{bmatrix} E_1 \\ E_2 \\ E_3 \end{bmatrix} \tag{I.25}$$

So, it suffices to know the states of the switches (E_1, E_2, E_3) delivered by the control block to calculate the output voltages of the inverter.

I.11 Simulation of the PMSM and interpretation of the results

I.11.1 simulink model

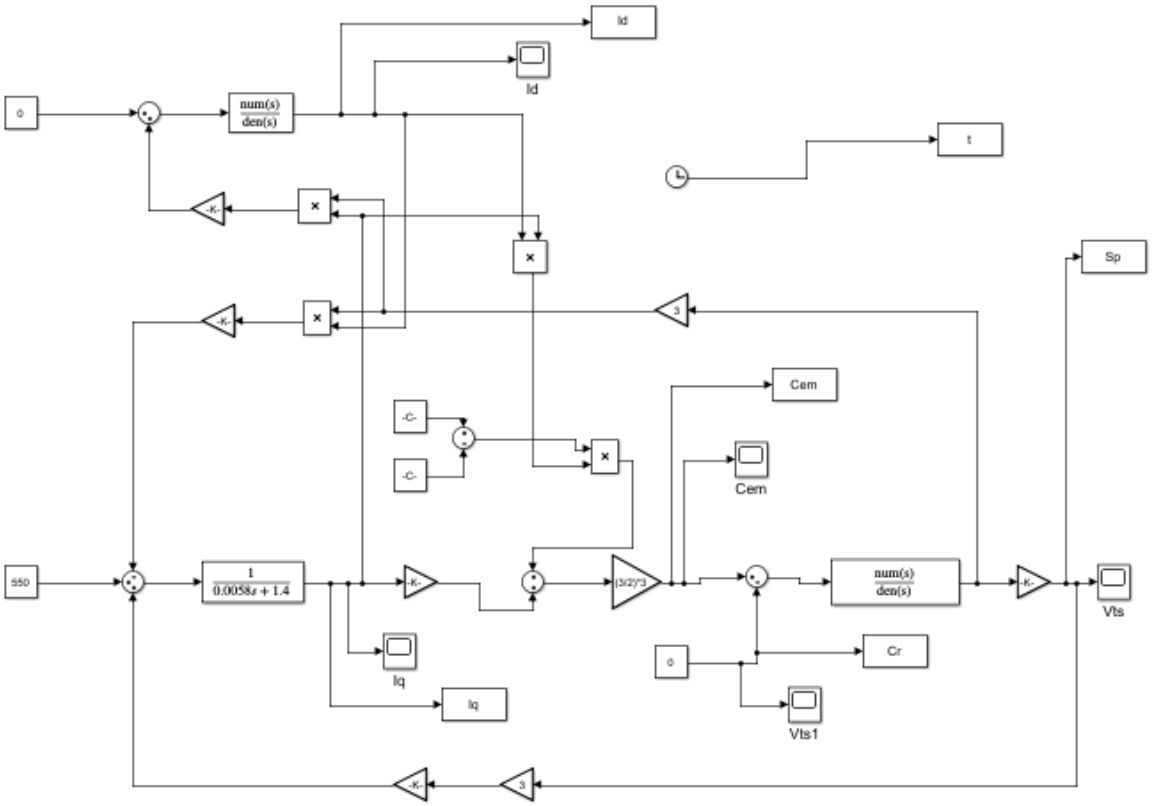

Figure I.9: PMSM block scheme.

I.11.2 Simulation results

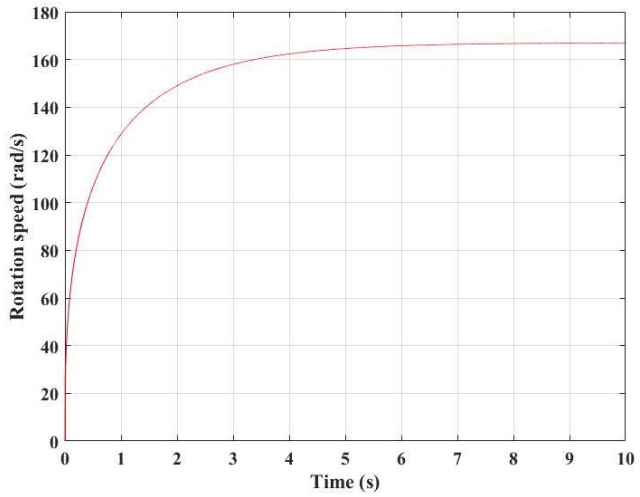

(a) Rotation speed

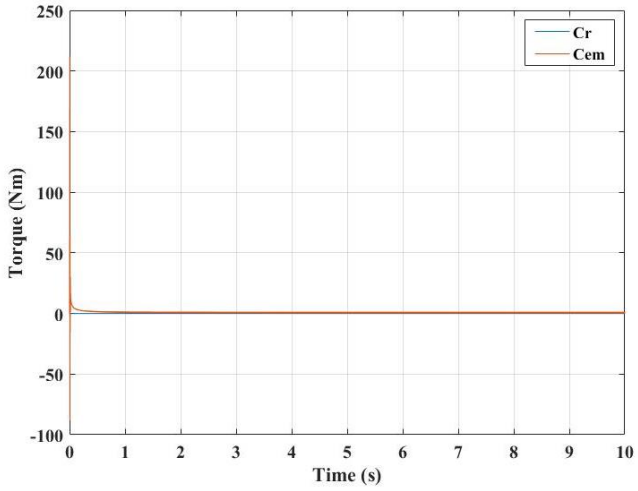

(b) Electromagnetic toque

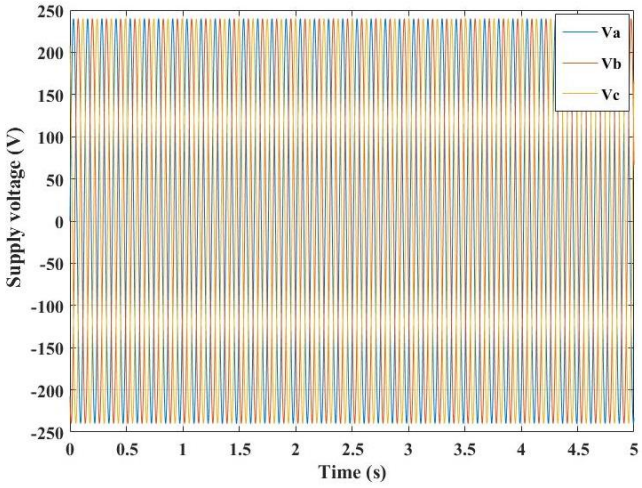

(c) Supply

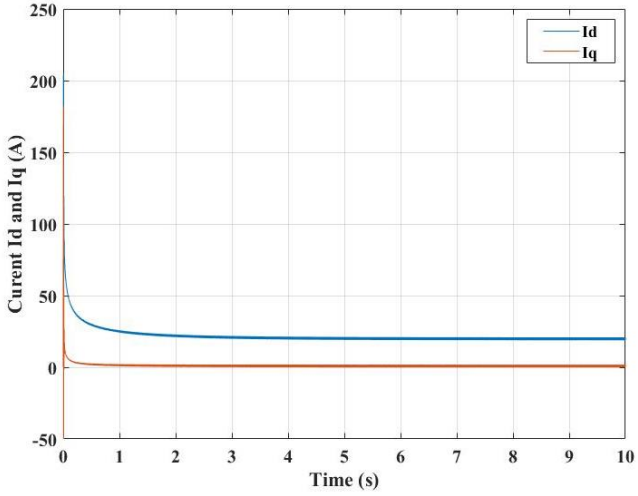

(d) Current Id and Iq

Figure I.10: Reselts of simulation

Discussion of results:

From Figure [I.10], it can be observed that during off-load startup, the motor speed precisely tracks its reference, achieving it rapidly. Additionally, the electromagnetic torque initiates at 10 N.m and eventually stabilizes at zero. It is noteworthy that the I_d component commences at 60 A and settles at 20 A, while the Iq current mirrors the torque behavior.

with load:

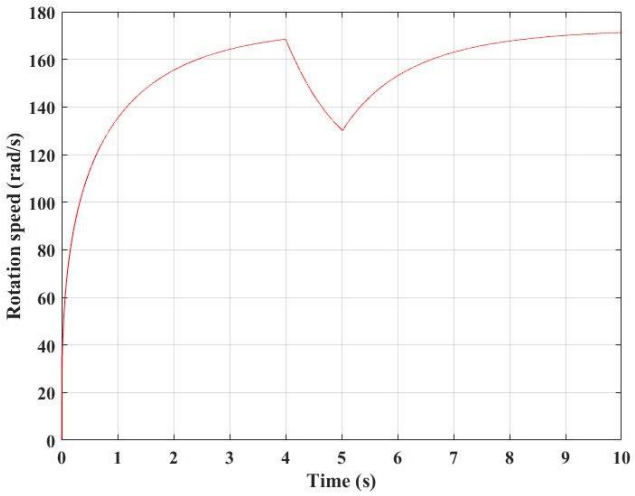

(a) Rotation speed

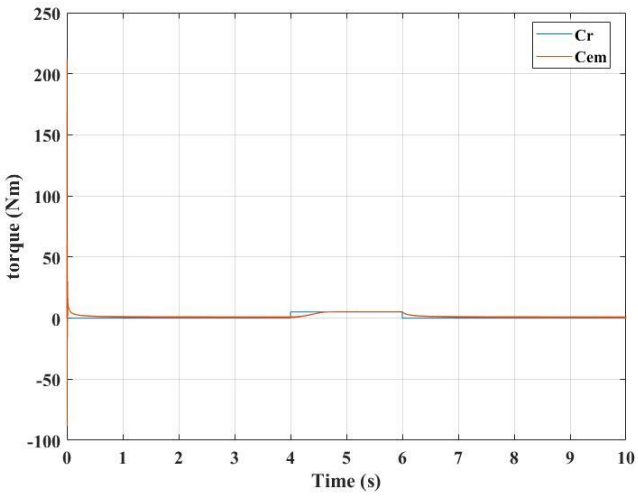

(b) Electromagnetic torque

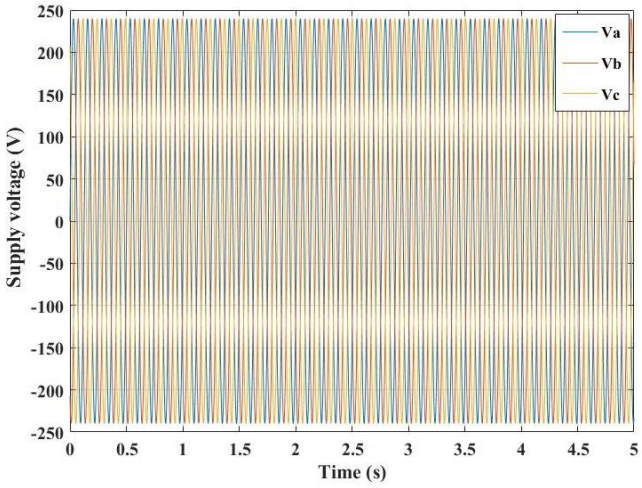

(c) Supply

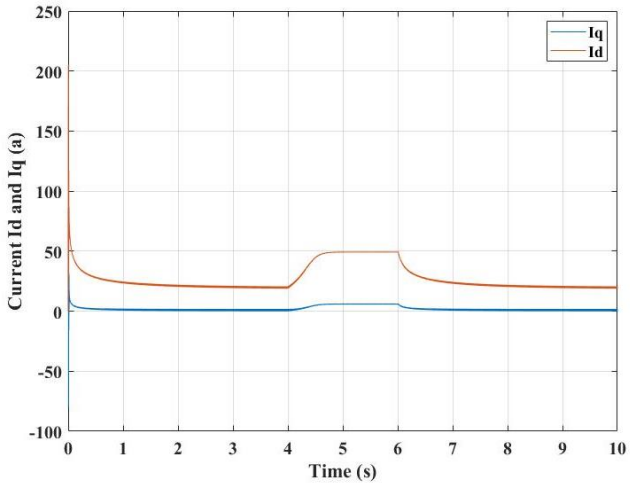

(d) Current Id and Iq

Figure I.11: Reselts of simulation

Discussion of results:

To analyze the impact of load on PMSM behavior, a torque load is applied to the motor along with a three-phase power supply.

it is observed that an increase in load causes the speed to decrease, but the speed quickly returns to stability within seconds. Regarding the electric torque and the two currents I_q and I_d, they have a positive effect, which is to increase each of them to a specific value and then return them to their initial stability within a few seconds.

I.12 Conclusion

in this chapter, we have become familiar with the permanent magnet synchronous motor, its essential components, operating methods, and working principle. Additionally, we have explored its mathematical model related to the transformer. The derived model is obtained by converting from three phases to two phases in two reference frames, one of which is fixed while the other rotates at the rotor speed.Lastly, we have conducted simulations of the motor under both unloaded and loaded conditions.

As the synchronous motor with permanent magnets always requires an association with a static converter during its operation, control of the converter is crucial in practice. The upcoming chapter will introduce one of these techniques, namely direct torque control.

Chapter II

Control of a PMSM by the DTC

II.1 Introduction

The Direct Torque Control (DTC) method was introduced in 1985 by Takahashi and Depenbrock for the purpose of torque control in high power servo motors. DTC is a control technique that takes advantage of the ability to independently regulate torque and flux in AC machines, achieved through a voltage inverter without the need for current regulation via a feedback loop.

In the subsequent discussion, our focus will be on the direct control of torque and flux. We will commence by introducing and implementing a control structure for the PMSM using DTC. Subsequently, we will present simulation results of the PMSM controlled by DTC and powered by a voltage inverter. These results will include scenarios both with and without a speed adjustment loop, implemented by a PI corrector.[21][22].

II.2 The Direct Torque Control (DTC)

The goal of the DTC is to directly control stator flux and linkage torque rather than to control stator current. This was achieved by directly controlling the power switches using hysteresis comparators and selecting voltage vectors from a predetermined switching table.

Depenbrock also proposed a similar control method in 1987, which he called Direct Autonomous Control (DSC). The term "direct torque control" (DTC) was later coined by Takahashi and Ohmori in a later paper. DTC gained popularity, and Tiitenen discussed its first industrial application. Since then, many papers have been published on various aspects of DTC for asynchronous motors, and there has been interest in applying DTC to permanent magnet synchronous motors.

The implementation of DTC in permanent magnet synchronous motors (PMSM) is discussed

by L. Zhong. In 1998, a DTC scheme was proposed to drive a wide speed range for an internal PMSM drive, which offers advantages over today's traditional field-of-control (FOC) drives. DTC control schemes have been proposed subsequently for internal permanent magnet (IPM) motors with approximately constant switching frequency.

In 2002, a completely sensorless DTC control of the IPM motor was proposed, which used a new speed estimator based on the stator flux correlation vector and torque angle. To reduce torque ripples, Sun proposed a fuzzy logic algorithm to improve the selection of voltage vectors. Today, DTC has become an accepted control method along with field control (FOC)[23].

II.3 General principles of DTC

DTC is a vector control method used to control the torque and therefore the speed of the motor bycontrolling the switching sequence of the inverter transistors. Figure II.1 shows the DTC for a PMSM block diagram. It can be seen that once one has the estimated and reference instantaneous values of electromagnetic torque and stator flux, we proceed to calculate the error between them, these errors are used as inputs for the hysteresis controllers, which aim to maintain the torque and flux errors within upper and lower limits allowed, so that when evaluating within these limits an output level is obtained to know the status of the variable. The output levels achieved in this stage of the control are input signals to the block that is responsible for finding the right vector to get rid of the speed error. This procedure is made for each sampling instant to drive the PMSM to the desired speed value[11].

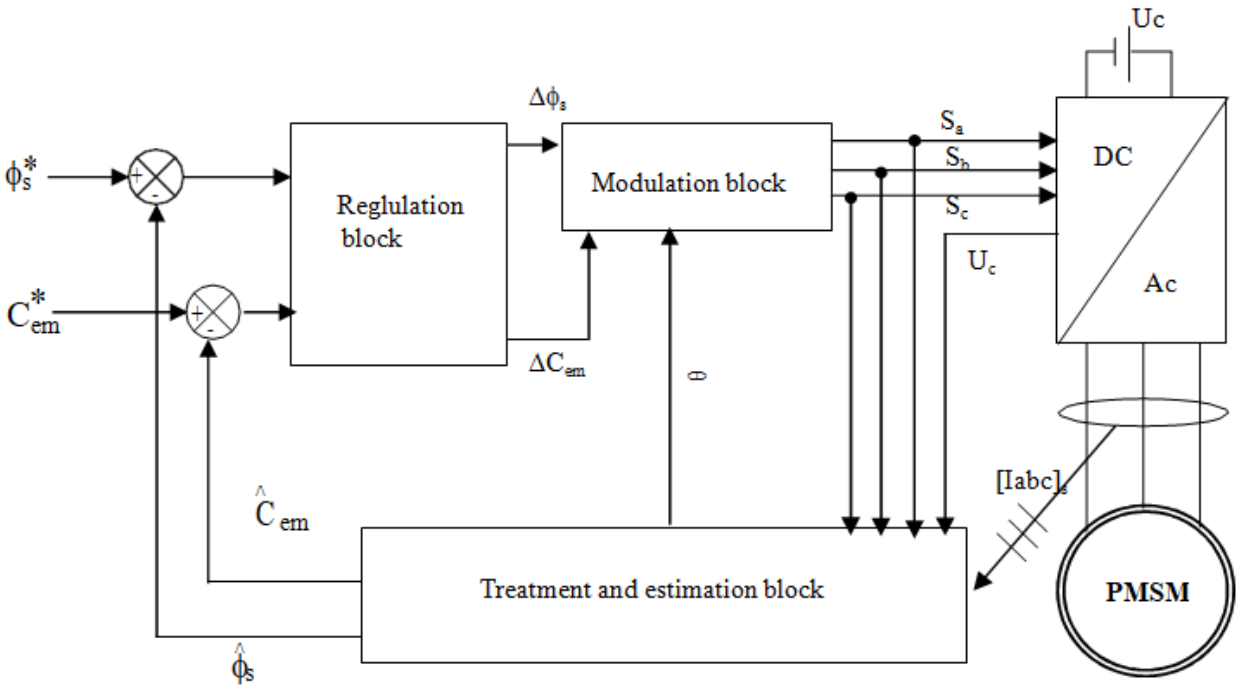

Figure II.1: Structural diagram of a DTC command applied to the PMSM.

In the DTC, the motor torque control is achieved with two hysteresis controllers, one for stator flux magnitude error and the other for the torque magnitude error. The selection of one switching vector per sampling time depends on the sign of these two controllers without inspections of the magnitude of the errors produced in the transient and dynamic situations per sampling time and level of the applied stator voltage[11].

II.4 Advantages and disadvantages of PMSM

II.4.1 Advantages

- Not to require calculations in the rotor reference frame (d,q).
- DTC does not require any current regulator, coordinate transformation and PWM signals generator (as a consequence timers are not required).
- In spite of its simplicity, DTC allows a good torque control in steady-state and transient operating conditions to be obtained.
- The dynamic response is very fast.[10][24]

II.4.2 disadvantages

- difficulty to control torque and flux at very low speed.
- high current and torque ripple.
- variable switching frequency behavior.
- high noise level at low speed.
- lack of direct current control.[10][24]

II.5 Direct control strategy of flux and torque

II.5.1 Stator flux vector control

We set a constant reference $\alpha\beta$ linked to the stator of the machine. The stator flux can be obtained by the following equation[25][8]:

$$\bar{V_s} = R_s\bar{I}s + \frac{d\bar{\phi_s}}{dt} \Rightarrow \bar{\phi_s} = \bar{\phi_{s0}} + \int_0^t (\bar{V_s} - R_s\bar{I}s)dt \tag{II.1}$$

Where: ϕ_{s0} is the flux vector at time t = 0

In this study we will consider the term $R_s\vec{I_s}$ negligible in front of the voltage vector $\vec{V_s}$ which is verified when the rotational speed is high enough. From the previous equation, we find :

$$\Delta\bar{\phi_s} = \bar{V_s}T_e \tag{II.2}$$

We see that over the time interval [0, T_e], the extremity of the vector $\bar{\phi_s}$ moves on a straight line whose direction is given by $\vec{V_s}$, figure (II-2).

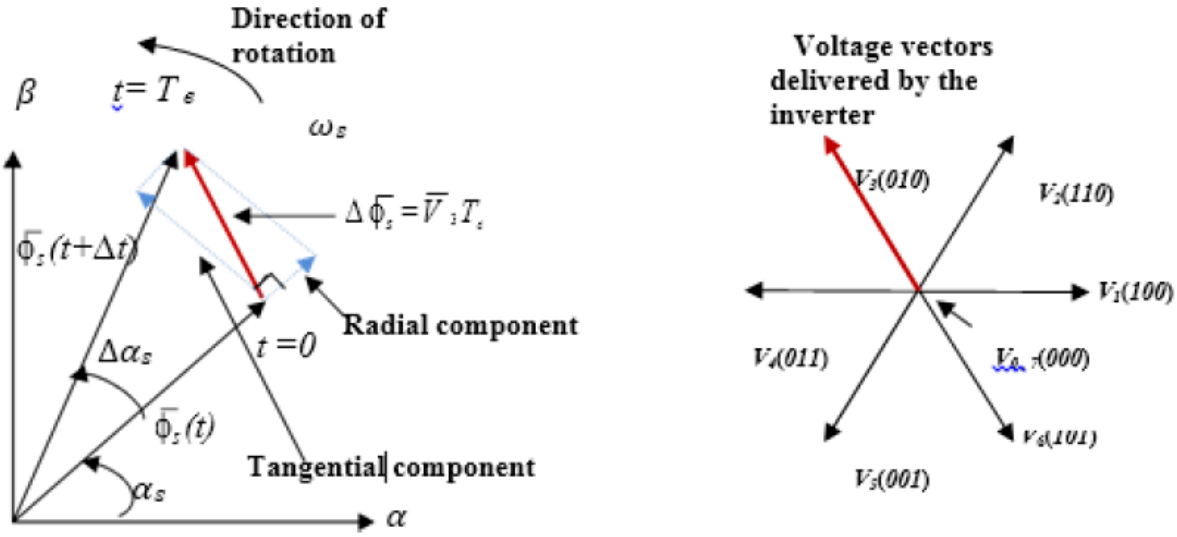

Figure II.2: Evolution of the end of $\vec{\phi_s}$ for negligible $R_s\vec{I_s}$.[8].

By implementing a suitable series of the vector $\bar{V}_s$ within consecutive time intervals of T_e, we can effectively steer the end of the vector $\bar{\phi}_s$ along the intended path. This allows us to maintain a consistent modulus of the $\bar{\phi}_s$ flux through automated means. To achieve this, it is necessary to trace an almost circular trajectory at the end of $\bar{\phi}_s$', provided that the duration T_e is significantly shorter than the stator flux rotation period T_s[8].

Note

In the case of PMSM, the stator flux continues to change even when the zero voltage vector is applied because the permanent magnets rotate with the rotor, Consequently the application of zero voltage vectors is to be avoided to control the stator flux. In other words, the stator flux must always be in motion relative to the rotor flux.[9]

II.5.2 Electromagnetic torque control

The electromagnetic torque is proportional to the vector product between the vectors of the stator and rotor fluxes in the following way.[26][9]

$$C_e = K(\bar{\phi}_s \times \bar{\phi}'_r) = K||\bar{\phi}_s|||\bar{\phi}'_r||sin(\delta) \tag{II.3}$$

where : $K = \frac{P}{L_q}$

with :

- $\bar{\phi}_s$: is the stator flux vector.
- $\bar{\phi}'_r$: is the rotor flux vector brought back to the stator.
- δ : is the angle between the stator and rotor flux vectors.

The torque therefore depends on the amplitude of the two vectors $\bar{\phi}_s$ and $\bar{\phi}'_r$ and their relative position, If one manages to perfectly control the flow $\bar{\phi}_s$ (from $\bar{V}_s$) in modulus and in position, we can therefore control the amplitude of $\bar{\phi}_s$, and the electromagnetic torque in a decoupled way.

II.6 Selection of Voltage Vectors

The choice of the stator voltage vector $\bar{V}_s$ depends on the desired variation for the stator flux modulus $\bar{\phi}_s$, the direction of rotation of $\bar{\phi}_s$, and the desired change for the torque.

By placing the one oneself in the stator frame $\alpha\beta$, one can delimit the space of $\bar{\phi}_{s0}$ by dividing it into six zones called sectors, which are determined from the flux components along the axes α and β. The axis α is chosen to coincide with the axis of the phase (a) of the three-phase winding (a, b, c) see figure(II.3)[7][27].

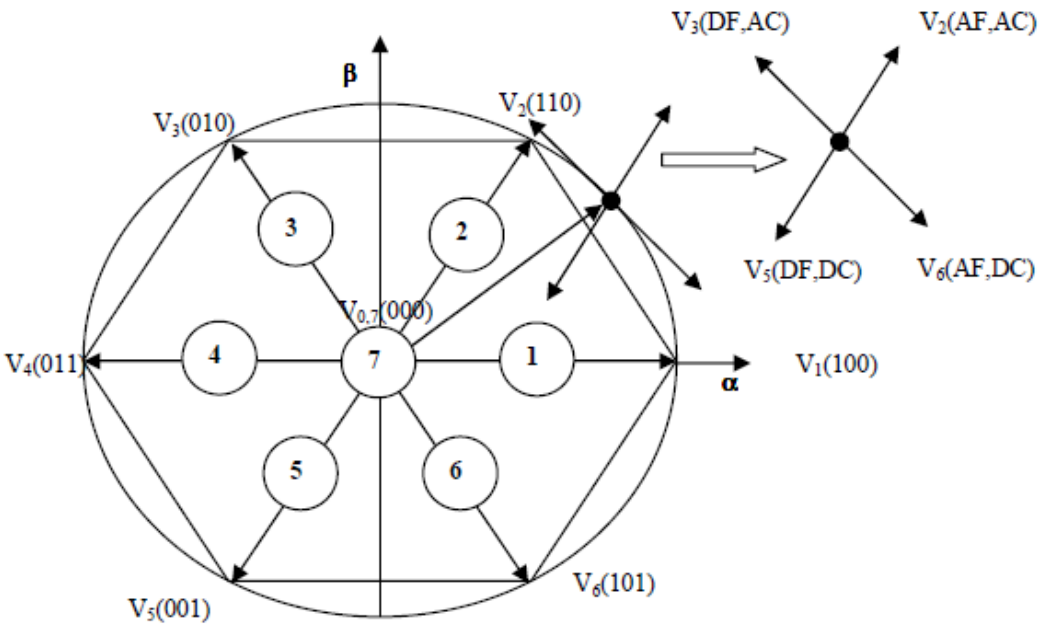

Figure II.3: distribution of the complex plane into six angular sectors[7]

.

$S_i = 1....6$

- AF : Increase flux
- AC : increase the torque
- DF : Decrease flux
- DC : Decrease the torque

When flux $\bar{\phi_s}$ is in zone i (i=1,.....6), flux and torque control can be provided by selecting one of the following eight voltage vectors.

- If $\bar{V_{i+1}}$ is selected, then $\bar{\phi_s}$ increases and C_{em} increases
- If $\bar{V_{i-1}}$ is selected, then $\bar{\phi_s}$ increases and C_{em} decreases
- If $\bar{V_{i+2}}$ is selected, then $\bar{\phi_s}$ decreases and C_{em} increases
- If $\bar{V_{i-2}}$ is selected, then $\bar{\phi_s}$ decreases and C_{em} decreases
- If $\bar{V_0}$ or $\bar{V_7}$ are selected, then the rotation of the $\bar{\phi_s}$ flux is stopped, hence a decrease in torque while the flux modulus $\bar{\phi_s}$ remains unchanged.

The efficiency of the voltage vectors applied also depends on the position of the stator flux vector in region i.

At the beginning of zone i, the vectors $\bar{V_{i+1}}$ and $\bar{V_{i-2}}$ are perpendicular to the flux vector, As a result their contribution to the flux is negligible, Consequently the torque change happens rapidly, and the amplitude of the flux remains relatively unchanged Additionally, at the same position the angles between $\bar{V_{i-1}}$ and $\bar{V_{i+1}}$ and the flux vector are 150° and 30° respectively, Consequently their contribution to the torque is very low. (Fig II.3)

The flux variations after the application of these two voltage vectors are significant and the torque changes are very small[7][27].

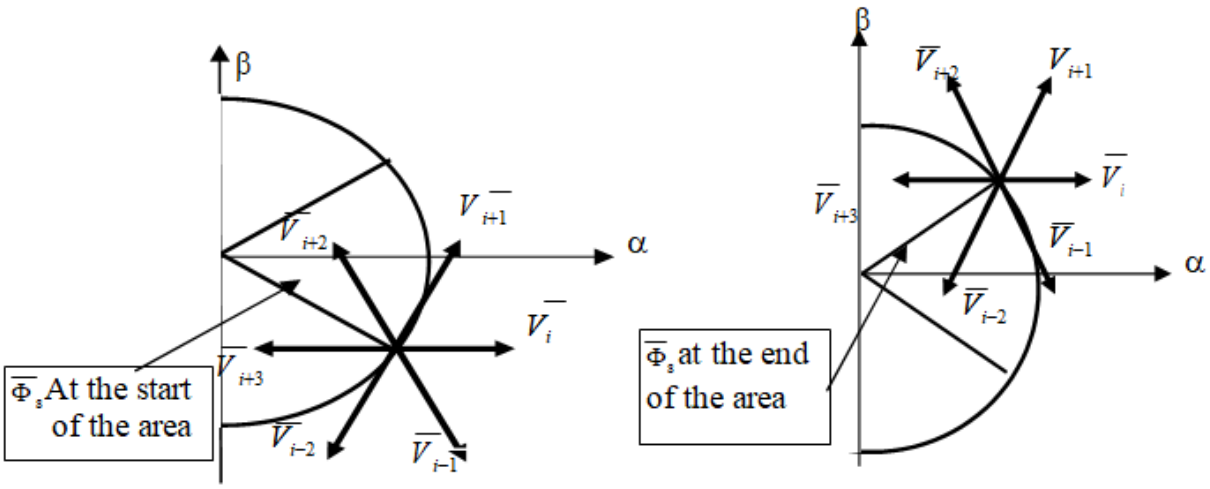

Figure II.4: Different effects of the tension vectors at the beginning and at the end of the zone[7]

.

II.7 Flux and Torque Estimation

II.7.1 Stator flux estimation

The estimation of the flux can be made from measurements of the stator quantities of the current and the voltage of the machine.

From the equation (II.1), we obtain the components α, β related to the stator of the vector $\bar{\phi}_s$.

$$\begin{cases} \hat{\phi_{s\alpha}} = \int_0^t (\bar{V_{s\alpha}} - R_s \bar{I_{s\alpha}})dt \\ \hat{\phi_{s\beta}} = \int_0^t (\bar{V_{s\beta}} - R_s \bar{I_{s\beta}})dt \end{cases} \tag{II.4}$$

The $V_{s\alpha}$ and $V_{s\beta}$ voltages are determined from the commands (T_a,T_b,T_c) from the measurement of the U_c voltage and by applying the Concordia transform:

$$\bar{V_{s\alpha}} = V_{s\beta} + jV_{s\beta} \tag{II.5}$$

$$\begin{cases} V_{s\alpha} = \sqrt{\frac{2}{3}} U_c (T_a - \frac{1}{2}(T_b + T_c)) \\ V_{s\beta} = \sqrt{\frac{1}{2}} U_c (T_b + T_c) \end{cases} \tag{II.6}$$

Similarly, the currents $I_{s\alpha}$ and $I_{s\alpha}$ are obtained from the measurement of the real currents I_{sa}, I_{sb} and I_{sc}, ($I_{sa} + I_{sb} + I_{sc} = 0$) and by application of Concordia's transformation:[10][28]

$$\bar{I}_s = I_{s\alpha} + jI_{s\beta} \tag{II.7}$$

$$\begin{cases} I_{s\alpha} = \sqrt{\frac{2}{3}} I_{s\alpha} \\ I_{s\beta} = \frac{1}{\sqrt{2}}(I_{sb} - I_{sc}) \end{cases} \tag{II.8}$$

The stator flux model is written :

$$\hat{\phi}_s = \sqrt{\hat{\phi_{s\alpha}}^2 + \hat{\phi_{s\beta}}^2} \tag{II.9}$$

The zone Ni in which the vector $\bar{\phi}_s$ is located is determined from the components $\hat{\phi_{s\alpha}}$ and $\hat{\phi_{s\beta}}$. The angle θ between the frame (α, β) is the vector$\bar{\phi}_s$ is equal to:

$$\hat{\theta} = Arctg \frac{\hat{\phi_{s\beta}}}{\hat{\phi_{s\alpha}}} \tag{II.10}$$

II.7.2 Electromagnetic torque estimation

The electromagnetic torque can be estimated from flux estimation and current measurement using the expression of torque as a function of flux and stator current given by the equation:

$$\hat{C_{em}} = P[\hat{\phi_{s\alpha}} I_{s\beta} - \hat{\phi_{s\beta}} I_{s\alpha}] \tag{II.11}$$

II.8 Elaboration of the command vector

II.8.1 The flux elaboration

The objective of this correction is to preserve the amplitude of the stator flux in a band and thus to maintain the end of the latter in a circular ring as shown in the figure (II-5).

The output of the corrector must indicate the direction of evolution of the module of the flux. The two thresholds of the comparator are chosen according to the ripple tolerated by the stator flux.[29][30]

We can then write :

$$\begin{cases} Si & \Delta\phi_s > \varepsilon_\phi \\ Si & 0 \leq \Delta\phi_s \leq \varepsilon_\phi \\ Si & 0 \leq \Delta\phi_s \leq \varepsilon_\phi \\ Si & \Delta\phi_s < -\varepsilon_\phi \end{cases} \text{ and } \begin{cases} \frac{d\Delta\phi_s}{dt} > 0 \\ \frac{d\Delta\phi_s}{dt} < 0 \end{cases} \begin{cases} So & K_\phi = 1 \\ So & K_\phi = 0 \\ So & K_\phi = 1 \\ So & K_\phi = 0 \end{cases} \tag{II.12}$$

$K_\phi = 0$ Meaning that the flux must be reduced.

$K_\phi = 1$ Meaning that the flux must be increased.

This two-level hysteresis regulator is ideal for good dynamic performance.

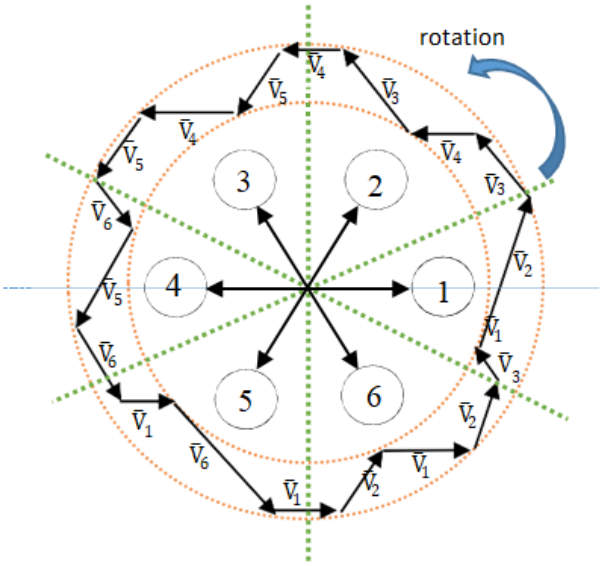

(a) Selection of voltages Vi to control flux

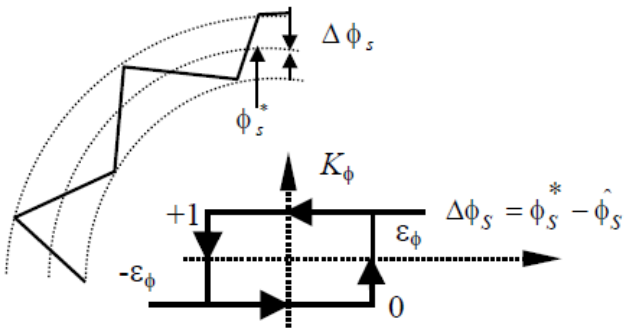

(b) Two-level hysteresis comparator for flux control

Figure II.5: the flux corrector[9]

II.8.2 The torque elaboration

The function of the torque corrector is to maintain the torque within the limits:

$$|C_e^* - \hat{C}_e| \leq \varepsilon_{C_e} \tag{II.13}$$

With :

C_e^* : The torque setpoint.

However, a difference with flux control is that the torque can be positive or negative depending on the direction of rotation of the machine. Two solutions can be considered:[22][6]

- a three-level hysteresis corrector
- a two-level hysteresis corrector.

The two-level corrector

This corrector is identical to the one used for the control of the $\bar{\phi}_a$ module. It only allows torque control in one direction of rotation. Thus only the $\bar{V_{k+1}}$ and $\bar{V_{k+2}}$ vectors can be selected to change the flux. Therefore, the decrease in torque is only achieved by the selection of null vectors. With this corrector, to reverse the direction of rotation of the machine, it is necessary to cross two phases of the machine. However, this corrector is easier to implement.

The three-level hysteresis corrector

The three-level hysteresis corrector (-1, 0, 1) makes it possible to control the motor in both directions of rotation, either for a positive or negative torque. This corrector is modeled by the algorithm (II.11), such that (Ccpl) represents the output state of the comparator and ε_{Ce} the limit of the hysteresis band (see figure II.6):[22][6]

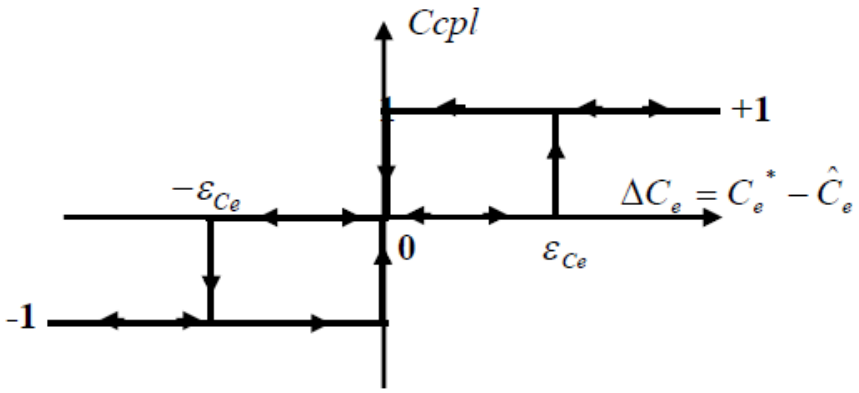

Figure II.6: Torque control from a three-level hysteresis corrector.[10]

$$\begin{cases} Si & \Delta C_e < \varepsilon_{C_e} \\ Si & 0 \leq \Delta C_e \leq \varepsilon_{C_e} \\ Si & 0 \leq \Delta C_e \leq \varepsilon_{C_e} \\ Si & \Delta C_e < -\varepsilon_{C_e} \\ Si & -\varepsilon_{C_e} \leq \Delta C_e < 0 \\ Si & -\varepsilon_{C_e} \leq \Delta C_e < 0 \end{cases} \text{ And } \begin{cases} \frac{d\Delta C_e}{dt} > 0 \\ \frac{d\Delta Ce}{dt} < 0 \\ \frac{d\Delta C_e}{dt} > 0 \\ \frac{d\Delta C_e}{dt} < 0 \end{cases} \text{ So } \begin{cases} Ccpl = 1 \\ Ccpl = 0 \\ Ccpl = 1 \\ Ccpl = -1 \\ Ccpl = 0 \\ Ccpl = -1 \end{cases} \quad \text{(II.14)}$$

By introducing the difference ΔC_e, between the reference electromagnetic torque C_e^* and that estimated $\hat{C}_e$ in a three-level hysteresis comparator, this generates the value (Ccpl=1) to increase torque, (Ccpl= -1) to reduce it and (Ccpl= 0) to keep it constant in a band ε_{C_e} around its reference. This choice to increase the number of levels is proposed in order to minimize the average switching frequency of the switches, because the torque dynamic is generally faster than the flux dynamic. In addition, this corrector allows a rapid decrease in the torque, in fact , to decrease the value of this one, in more of the null vectors (stopping of the rotation of $\bar{\phi}_s$), for example one can apply the vectors $\bar{V_{k-1}}$ or $\bar{V_{k-2}}$, if one chooses a direction of positive rotation (trigonometric direction). In this case, the flux $\bar{\phi}_r$ will catch up all the more quickly with the flux $\bar{\phi}_s$ that the latter is not satisfied only with "waiting for it: case of the applications of zero vectors" but " goes to meet it: inversion of the direction of rotation of $\bar{\phi}_s$.[10, 6, 27]

II.9 Elaboration of the switching table

The truth table is developed based on the errors of the flux and the torque $\Delta\phi_s$ and ΔC_e, and according to the position of the stator flux vector (N=1,..,6). The division of the complex plane into six angular sectors according to the figure (II-3) makes it possible to determine, for each given sector, the control sequence of the switches of the inverter which corresponds to the different states of the control quantities $\Delta\phi_s$ and ΔC_e following the logic of flux and torque behavior with respect to the application of a stator voltage vector.[6, 7]

The table (II.1) summarizes the combined action of each configuration on the stator flux and the electromagnetic torque

	INCREASE	DECREASE
ϕ_s	V_{i-1}, V_i, V_{i+1}	V_{i+2} V_{i+3}, V_{i-2}
C_e	V_{i+1}, V_{i+2}	V_{i-1}, V_{i-2}

Table II.1: Switch table

The tables below generally summarize the active voltage sequences to be applied to increase or decrease the stator flux modulus and the electromagnetic torque depending on the sector.

Finally, the comparison of the control tables of the module of the stator flux and the electromagnetic torque allows the final synthesis of a single control table, but it can be broken down into two other tables, the first with zero voltage vectors and the second with vectors active voltage:

	N=1	N=2	N=3	N=4	N=5	N=6
$\phi_s \uparrow$	V_6, V_1, V_2	V_1, V_2, V_3	V_2, V_3, V_4	V_3, V_4, V_5	V_4, V_5, V_6	V_5, V_6, V_7
$\phi_s \downarrow$	V_3, V_4, V_5	V_4, V_5, V_6	V_5, V_6, V_1	V_6, V_1, V_2	V_1, V_2, V_3	V_2, V_3, V_4

Table II.2: Flux control table

	N=1	N=2	N=3	N=4	N=5	N=6
$C_e \uparrow$	V_6, V_1	V_1, V_2	V_2, V_3	V_3, V_4	V_4, V_5	V_5, V_6
$Ce \downarrow$	V_3, V_4	V_4, V_5	V_5, V_6	V_6, V_1	V_1, V_2,	V_2, V_3

Table II.3: Torque control table

Flux	toque	N=1	N=2	N=3	N=4	N=5	N=6	Corrector
	Ccpl=1	V_3	V_4	V_5	V_6	V_1	V_2	Level 2
$K_\phi = 0$	Ccpl=0	V_0	V_7	V_0	V_7	V_0	V_7	Level 2
	Ccpl=-1	V_5	V_6	V_1	V_2	V_3	V_4	Level 3
	Ccpl=1	V_2	V_3	V_4	V_5	V_6	V_1	Level 2
$K_\phi = 1$	Ccpl=0	V_7	V_0	V_7	V_0	V_7	V_0	Level 2
	Ccpl=-1	V_6	V_1	V_2	V_3	V_4	V_5	Level 3

Table II.4: Control strategy with three-level hysteresis comparator with zero voltage vectors

By selecting one of the zero vectors, the rotation of the stator flux is stopped and also causes a decrease in torque, we choose V_0 or V_7 so as to minimize the number of switching times of the same switch of the inverter

Flux	Toque	N=1	N=2	N=3	N=4	N=5	N=6	Corrector
	Ccpl=1	V_3	V_4	V_5	V_6	V_1	V_2	Level 2
$K_\phi = 0$	Ccpl=0	V_4	V_5	V_6	V_1	V_2	V_3	Level 2
	Ccpl=-1	V_5	V_6	V_1	V_2	V_3	V_4	Level 3
	Ccpl=1	V_2	V_3	V_4	V_5	V_6	V_1	Level 2
$K_\phi = 1$	Ccpl=0	V_1	V_2	V_3	V_4	V_5	V_6	Level 2
	Ccpl=-1	V_6	V_1	V_2	V_3	V_4	V_5	Level 3

Table II.5: Control strategy with three-level hysteresis comparator with non-zero voltage vectors.

II.10 General structure of the DTC applied to the PMSM

Figure (II-7) shows the general structure of the direct torque control of a permanent magnet synchronous machine fed by a voltage inverter. At each sampling period T_e, the stator flux and the

electromagnetic torque are estimated from the measurement of the stator currents and knowledge of the imposed voltage vector. The speed of rotation is measured by the sensor, compared with a reference, the error of this comparison passes through a PI type regulator to build the torque reference.

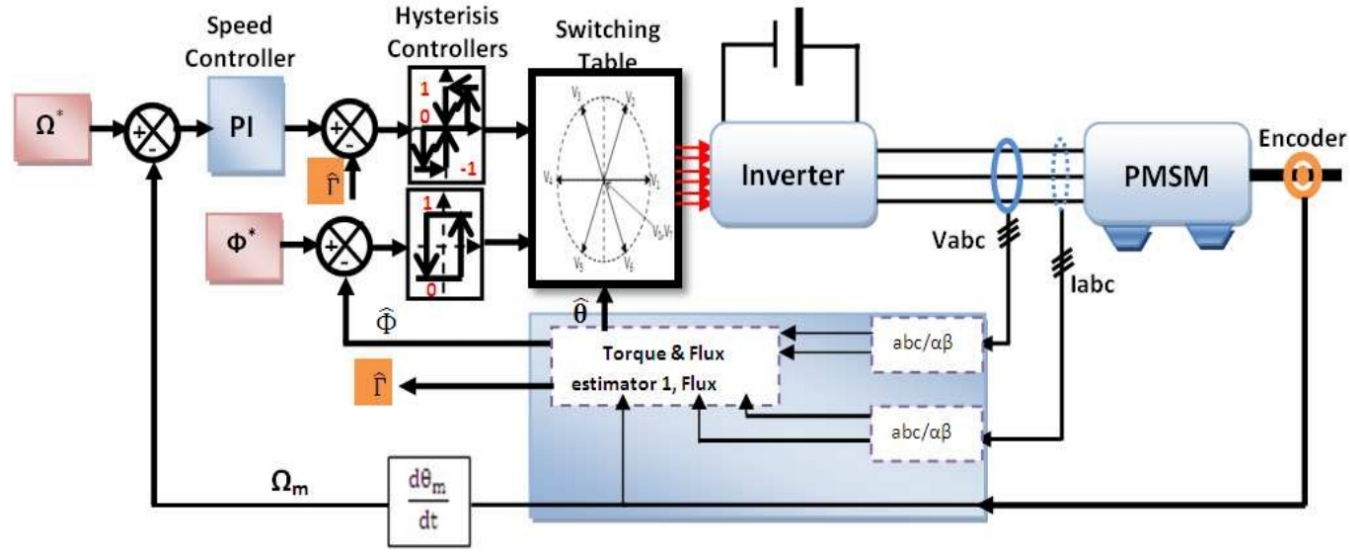

Figure II.7: Diagram of the general structure of the direct torque control of the PMSM.[11]

II.11 Simulation results

Using matlab simulation software, to illustrate the behavior of a DTC control architecture applied to an PMSM model powered by a three phase voltage inverter, in the presence of a speed tuning loop by a PI corrector.

Figures (I-8.I.9) represent the simulation results obtained from conventional DTC control with no load, and then input load torque Cr = 5 Nm at t = 0.1 s. there The motor runs at 100 rad/sec.

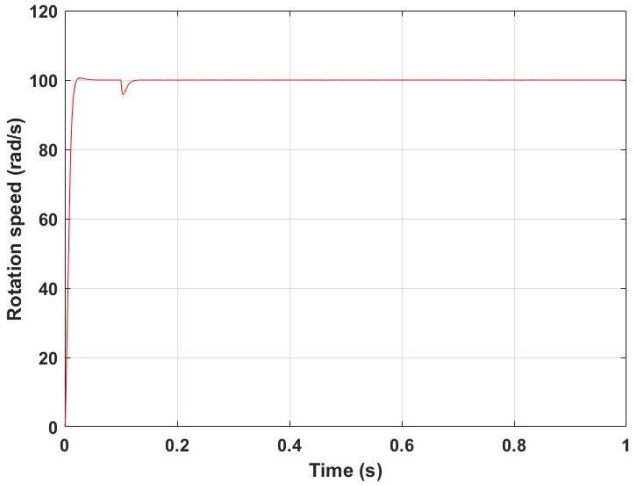

(a) Rotation speed

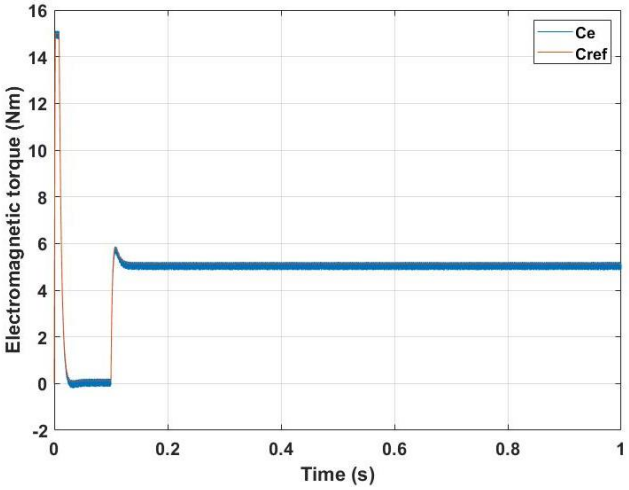

(b) Electromagnetic torque

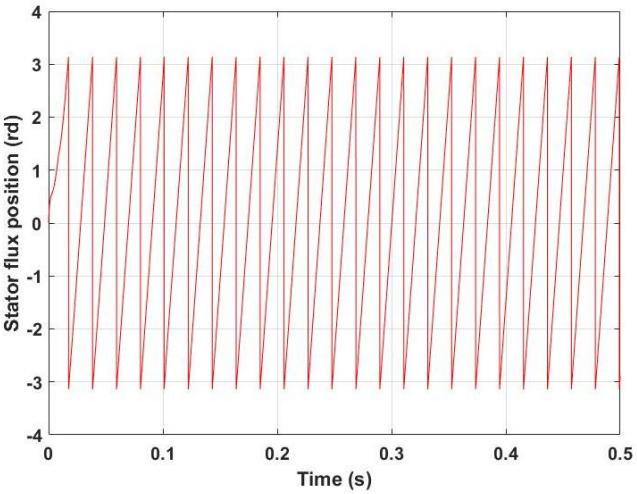

(c) Stator flux position

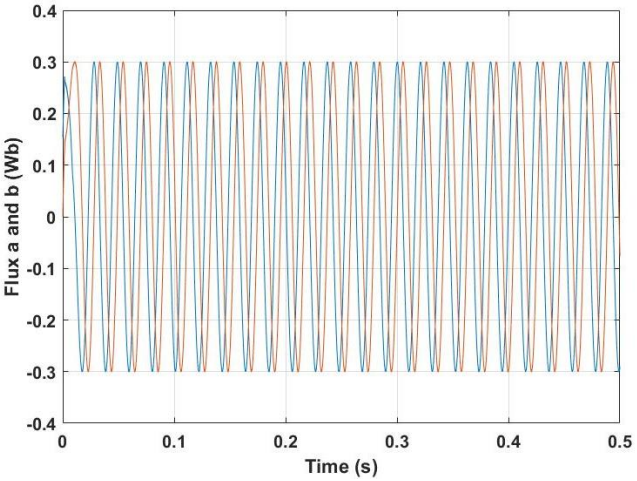

(d) Flux α and β

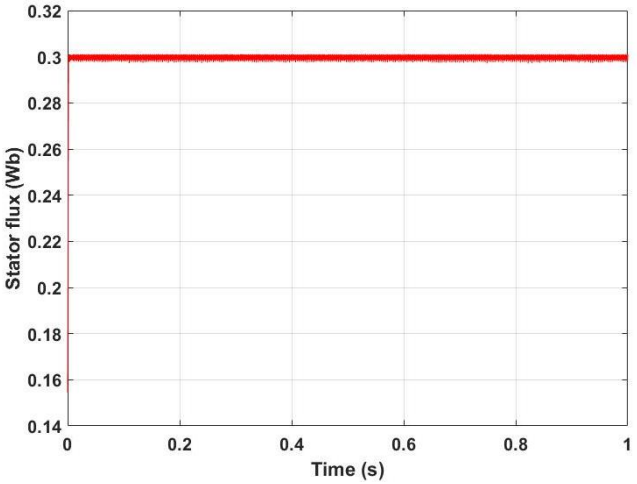

(e) Stator flux

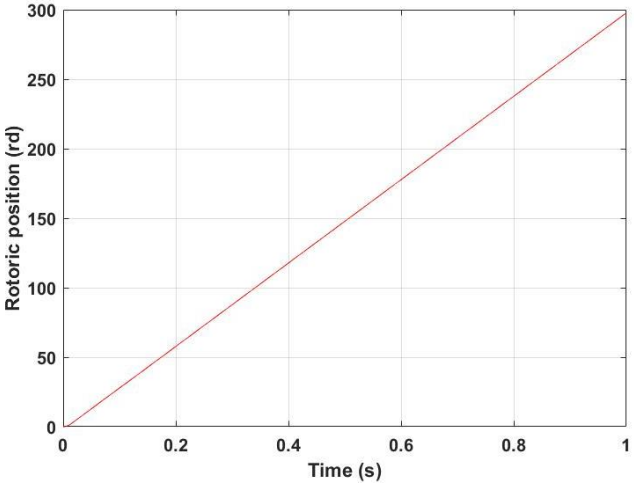

(f) Rotoric position

Figure II.8: Results of simulation

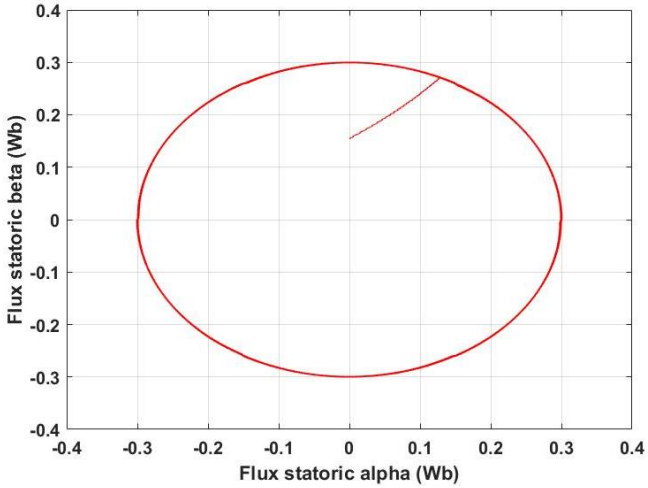

(a) Evolution of stator flux ($\phi_{\alpha s}, \phi_{\beta s}$)

Figure II.9: Results of simulation

Results interpretation

In this simulation case, we observe that the torque precisely tracks the setpoint value of the load with minimal impact on the speed, which quickly returns to its reference. This demonstrates that the DTC exhibits high dynamic performance without overshooting during startup.

Additionally, we notice that the flux remains unaffected by the load change.

Speed change test

To further evaluate the control's robustness regarding variations in the speed reference, a change in the speed setpoint from 100 rad/s to 120 rad/s is introduced at t = 0.25s, following a start-up under load. These results are depicted in the following figures:

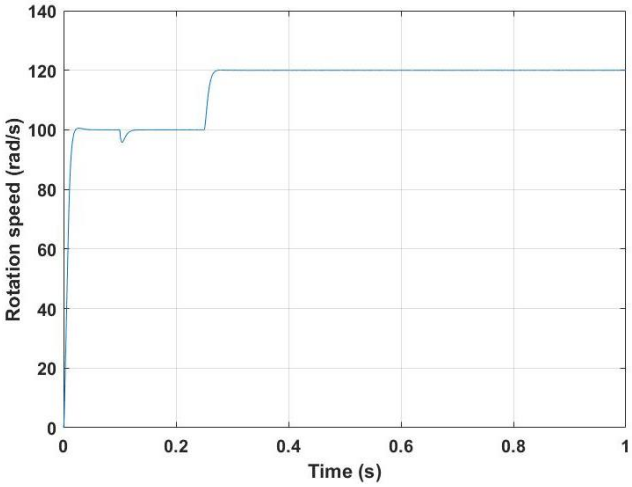

(a) Rotation speed

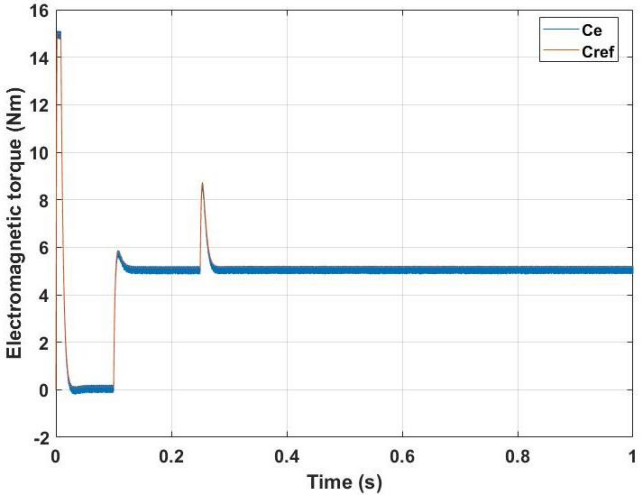

(b) Electromagnetic torque

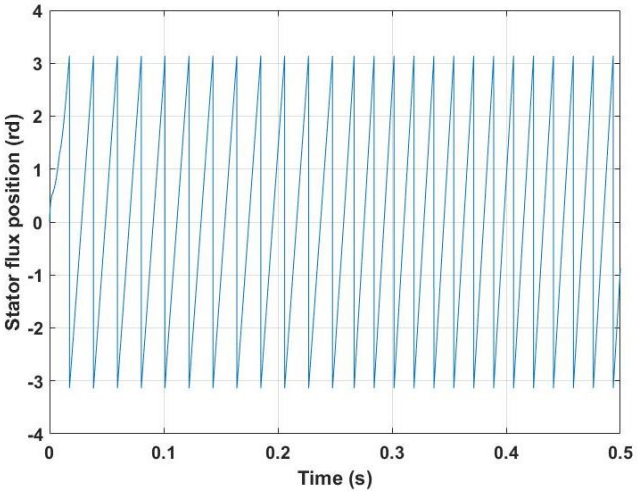

(c) Stator flux position

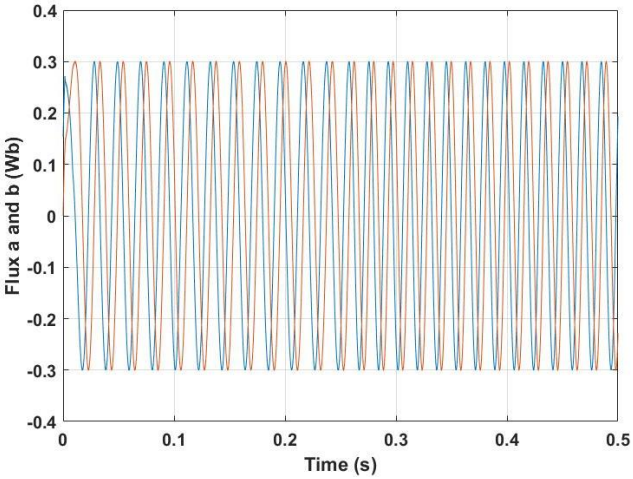

(d) Flux α and β

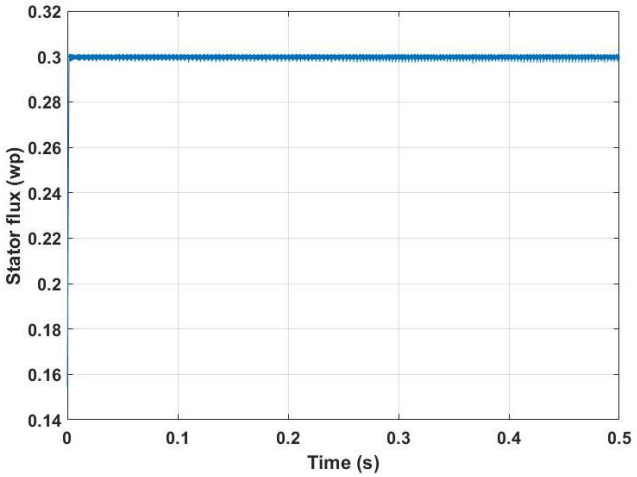

(e) Stator flux

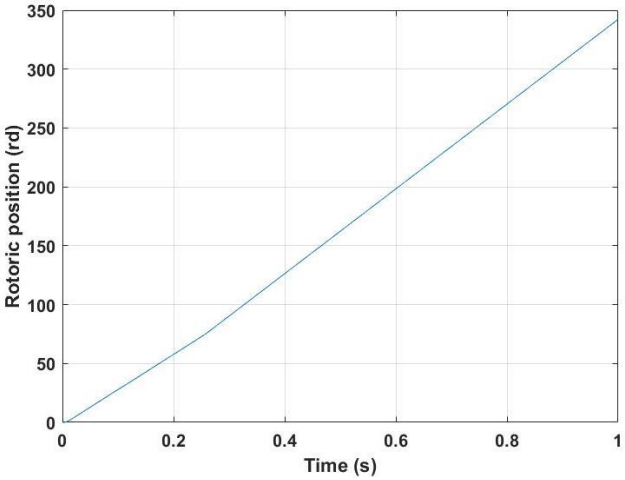

(f) Rotoric position

Figure II.10: Reselts of simulation

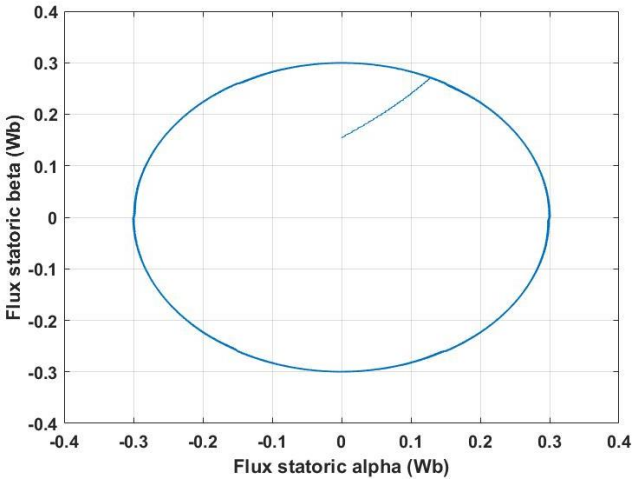

(a) Evolution of stator flux ($\phi_{\alpha s}, \phi_{\beta s}$)

Figure II.11: Reselts of simulation

Results interpretation

We observe that the system responds positively to this test. The speed tracks the new reference without any static error.The electromagnetic torque stabilizes near the load value and then increases after 0.25s, corresponding to the application of the speed reference variation. It eventually stabilizes at 5 N.m.

Another test to evaluate the control's robustness in relation to variations in the reference speed involved a change in the speed set point from 100 rad/sec to -100 rad/sec. In other words, we tested a rotation in the opposite direction under the same load. The corresponding results are depicted in the following figures.

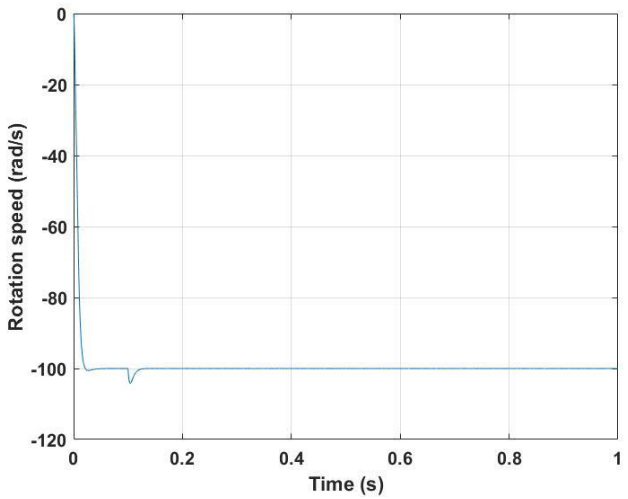

(a) Rotation speed

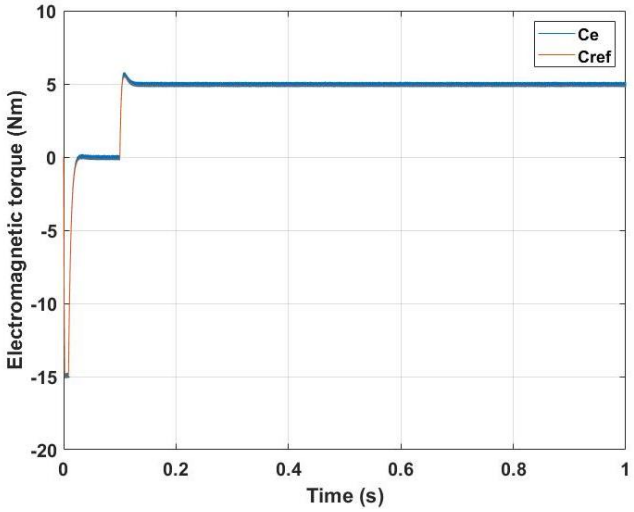

(b) Electromagnetic torque

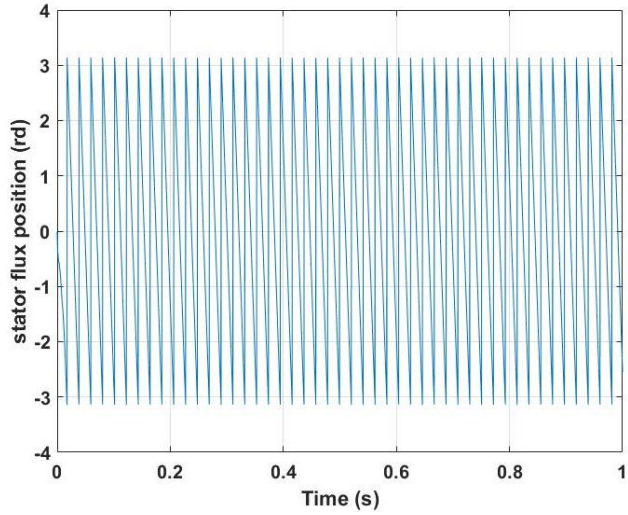

(c) Stator flux position

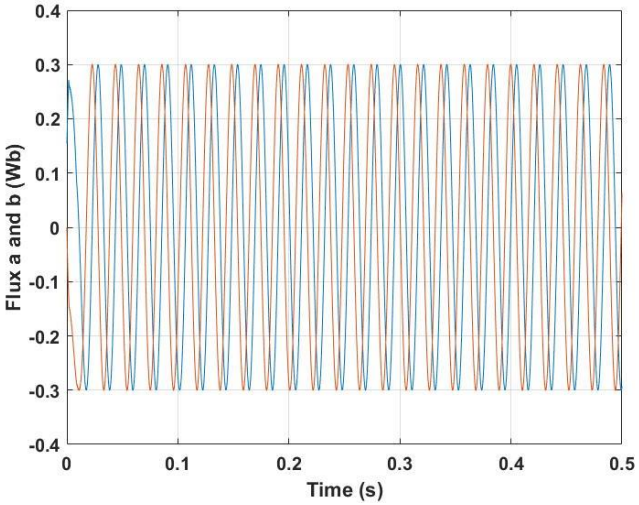

(d) Flux α and β

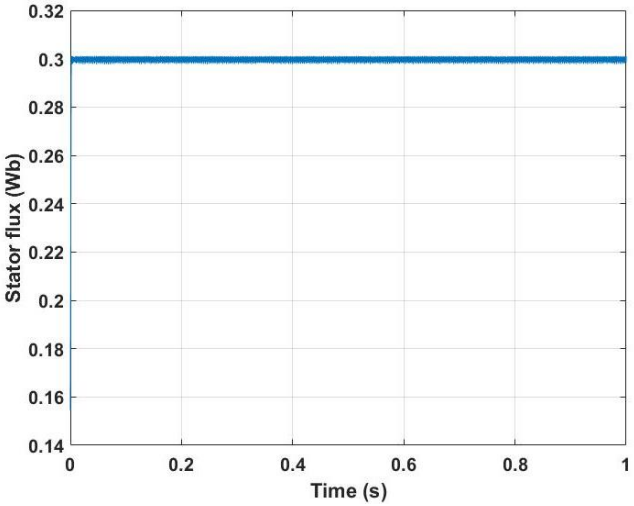

(e) Stator flux

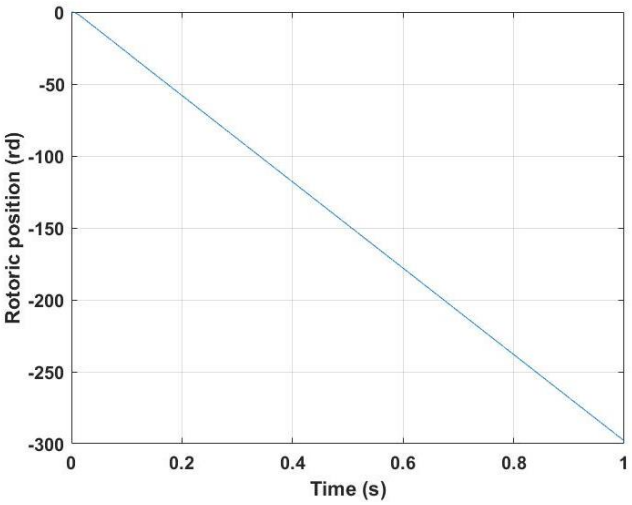

(f) Rotoric position

Figure II.12: Results of simulation

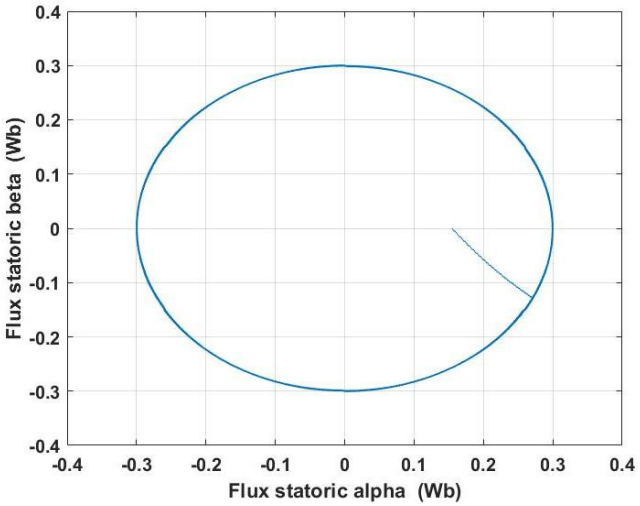

(a) Evolution of stator flux ($\phi_{\alpha s}, \phi_{\beta s}$)

Figure II.13: Reselts of simulation

Results interpretation

In this test, it is observed that the system effectively responds to the given scenario. It successfully tracks the new reference speed without any steady-state error. The electromagnetic torque stabilizes close to the load value, initially starting from a negative value of -15 Nm, which is in accordance with the applied velocity reference and load. Eventually, it settles at 5 Nm.

II.12 Conclusion

In this chapter, we have presented the structure of Direct Torque Control (DTC), which proves to be an efficient and straightforward method for driving a Permanent Synchronous Motor (PMSM). It provides a compelling solution to the control challenges and dynamics encountered.

We examined a DTC control structure powered by a voltage inverter and simulated the behavior of the PMSM with the inclusion of a PI corrector. It can be concluded that this control strategy demonstrates robustness against variations in machine parameters.

In summary, DTC exhibits commendable performance in terms of both dynamic and static torque and flux. Consequently, it offers a promising solution to address the issue of robustness.

Chapter III

The photovoltaic generator

III.1 Introduction

photovoltaic generator, also known as a solar generator, converts sunlight into electrical energy using photovoltaic cells. It is a clean and renewable energy solution that doesn't emit greenhouse gases. The generator consists of interconnected solar cells that absorb photons and generate an electric current through the photovoltaic effect. The generated electricity can be used immediately or stored for later use.

Photovoltaic generators are used in various applications, from residential rooftop systems to large-scale solar farms. They are environmentally friendly and help reduce reliance on fossil fuels. The efficiency and power output of the generator depend on factors like sunlight intensity, temperature, and shading. Proper design and maintenance are crucial for optimal performance. With advancing technology, photovoltaic generators are becoming more efficient and cost-effective, making solar energy an increasingly viable option for electricity generation.

III.2 Photovoltaic array systems and applications

Photovoltaic (PV) systems can be grouped into stand-alone systems and grid connected systems. In stand-alone systems the solar energy yield is matched to the energy demand. Since the solar energy yield often does not coincide in time with the energy demand from the connected loads, additional storage systems (batteries) are generally used. If the PV system is supported by an additional power source for example, a wind or diesel generator - this is known as a photovoltaic hybrid system. In grid-connected systems the public electricity grid functions as an energy store.

Small individual power supplies for homes, known as solar home systems, provide power for lights, radio, television, refrigerators, or pumps. Increasingly, villages are obtaining their own power supplies with an alternating current circuit and outputs in the two-digit kilowatt range.[31]

III.3 Classification of photovoltaic systems

In general, PV systems are classified into two groups: Stand-alone (off-grid) PV systems and grid-connected systems.

III.3.1 Stand alone systems

Stand-alone systems are typically implemented in rural and remote areas. They are usually supported by storage systems (e.g. batteries) in order to satisfy the load at times when the solar illuminance is not sufficient for the PV to cover all the need.

This type is particularly suitable for remote areas where basic energy needs are limited. Stand-alone systems mainly consist of a PV generator, a battery bank for storage and a set of static DC-DC and DC-AC converters. (See figure III.1).[32]

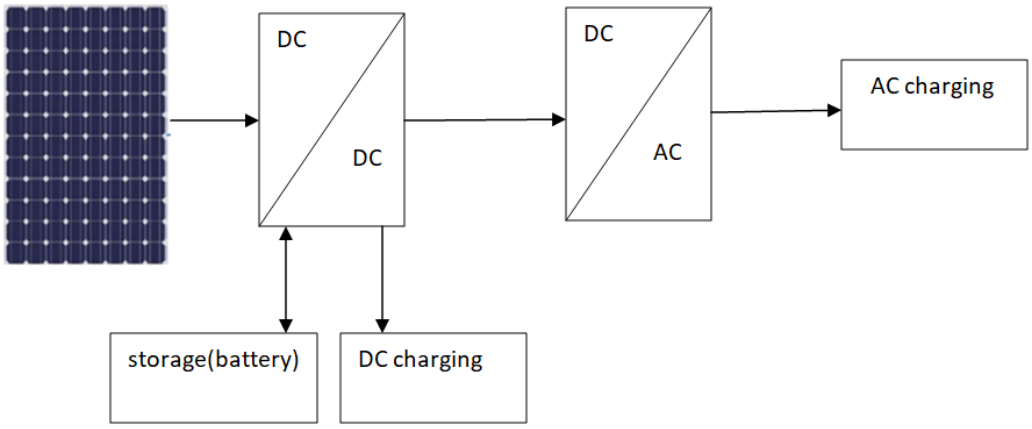

Figure III.1: Autonomous systems scheme.

III.3.2 Grid connected systems

Grid-connected systems are photovoltaic systems that are connected to distribution nodes and supply electricity to it. The connection is made via an inverter which converts direct current into alternating current and also ensures synchronization with the network in voltage and frequency. These systems can be connected directly to the public network or to the home network (Smart home). In general, there is no energy storage introduced on the grid side (See figure III.2).[32]

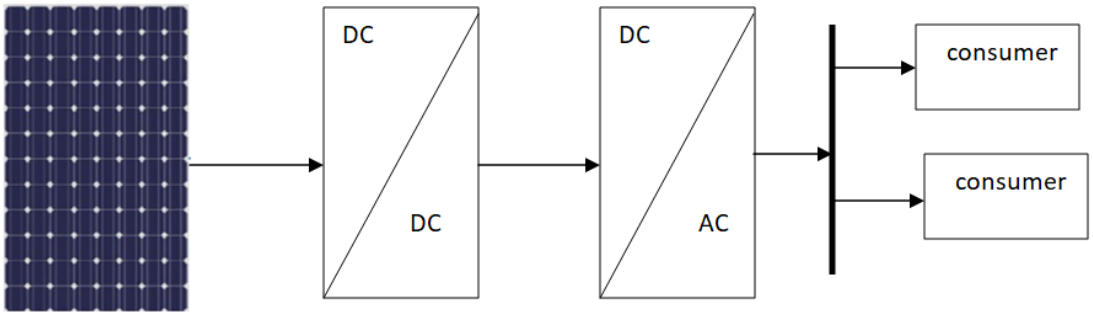

Figure III.2: Grid-connected PV system scheme.

III.4 PV generator

A photovoltaic generator(PVG), also known as a solar generator, is a device that converts sunlight directly into electrical energy using photovoltaic (PV) cells. PV cells are made of semiconductor materials, typically silicon, which can absorb photons (particles of light) and generate an electric current as a result of the photovoltaic effect.

The "PV" cell is approximately 150 cm2 and produces 2.3 Watt-peak W_P at around 0.5 Volt. This low power is generally insufficient for the majority of domestic or industrial PV applications. To provide the outdoor receiver with adequate voltage and power, several PV cells must be connected together in series to form what is called "a module." The modules can be assembled in series and/or in parallel to form panels, which are then interconnected to create a PV field.[13, 33]

Typically, $12V$ PV modules are used, consisting of 36 cells. A square meter of solar panels can generate up to $150W$. The amount of energy a module can supply depends on its surface area, temperature, and solar radiation. The voltage supplied by a module depends on the number of cells connected in series. For small power modules, the voltage is usually between 12V and $15V$. . The operating voltage can then reach $24V$ or more, depending on the power supply system configuration. Assembling modules in series and/or parallel enables adjustment of different voltages and powers. The characteristic of a PV cell is similar to that of a photo-diode but in generative agreement [13]

III.5 PVG-load connection

III.5.1 Direct connection

The direct connection of the photovoltaic solar panel to a load is the most economical and widely used operating principle. The operating point of the photovoltaic generator (PVG) depends on the impedance of the connected load, determined by the intersection between the I-V characteristic of the PVG and the I-V characteristic of the load. To prevent the flow of negative current to the PVG, an anti-return diode must be installed, as shown in the figure(III.3).[31, 12]

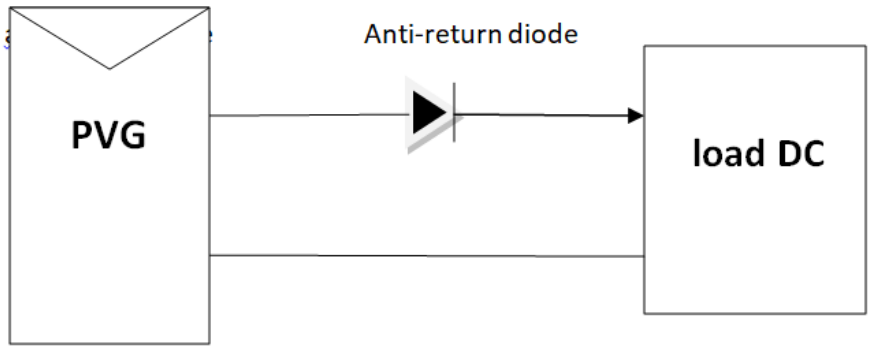

Figure III.3: PVG-Load direct connection

However, this configuration does not provide any means of limiting or adjusting the load voltage. Consequently, the transfer of the maximum available power from the PVG to the load is not guaranteed, as illustrated in the figure(III.4).

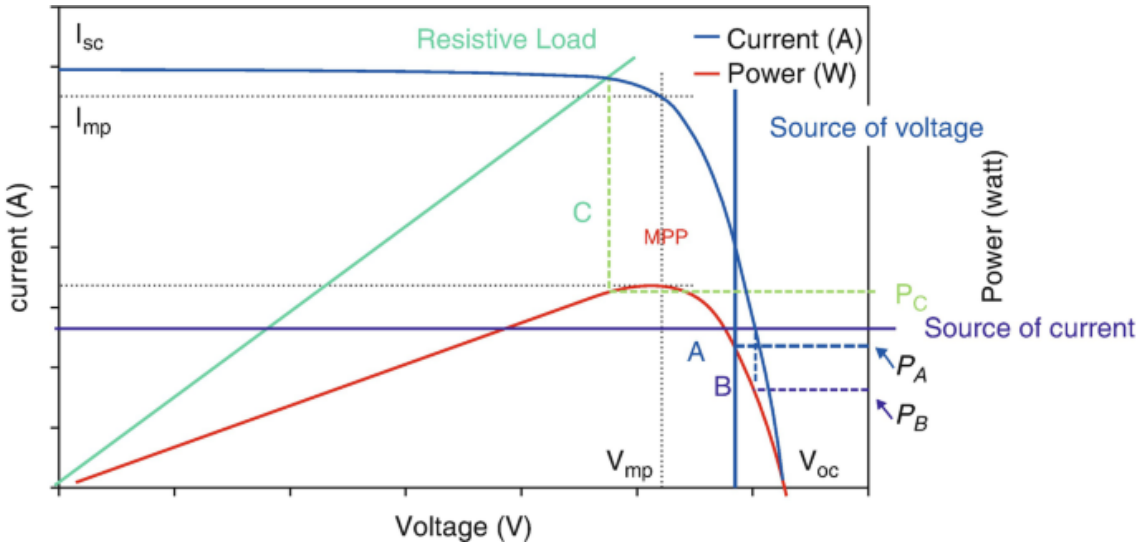

Figure III.4: Operating points of a PVG according to the load in direct connection.[12]

As depicted in the figure, there are three types of loads that can be directly connected to a PVG:

- A load of the DC voltage source type
- A load of the direct current source type
- A purely resistive load

At operating points A, B, and C, the power supplied by the generator is P_A, P_B, and P_C, respectively, all of which are lower than the maximum power P_{MAX}. The power difference is therefore lost and dissipated as heat in the generator. Additionally, some loads require an alternating

voltage source, whereas the PVG only provides direct current. Hence, direct connection is not possible in such cases. Consequently, the use of direct connection is limited due to the associated production losses and its applicability to devices operating solely on direct current.[31, 12]

III.5.2 Connection via an adaptation stage

PV generators their power production is influenced by factors such as illumination, temperature, and system aging. In direct connection mode, the actual power transferred to the load can differ significantly from the generator's potential power, depending on the load's characteristics.

To consistently achieve maximum power transfer, an adaptation stage is employed between the PV generator and the load. This stage, depicted in Figure (III.5), acts as an interface and utilizes control measures to ensure the transfer of the generator's maximum power to the load, regardless of weather conditions.

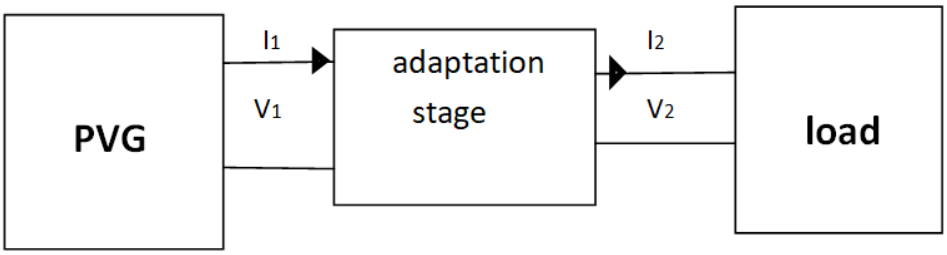

Figure III.5: Connecting a GPV to a load through an adaptation stage.

III.6 Modeling of a photovoltaic cell

To develop an equivalent model of a photovoltaic cell, it is necessary to make a judicious choice of the electrical circuits which constitute it and to understand the physical configuration and the electrical characteristics of the elements of the cell. For this, several mathematical models are developed to represent the nonlinear behavior of semiconductor junctions. In the following we present two models of a photovoltaic cell, namely the two-diode model and the one-diode model. Both are based on Shockley's well-known diode equation.[31, 34]

The characteristics of a photovoltaic cell will be described as follows:

- The short-circuit current (Isc) which supplies each cell is:

  $$I_{cc}(cell) = \frac{I_{cc}}{N_p} \tag{III.1}$$

- The open circuit voltage (Vco) that supplies each cell is:

  $$V_{co}(cell) = \frac{V_{co}}{N_s} \tag{III.2}$$

- The maximum current of each cell is:

$$I_{mp}(cell) = \frac{I_{mp}}{N_p} \tag{III.3}$$

- The maximum voltage of each cell is:

$$V_{mp}(cell) = \frac{V_{mp}}{N_s} \tag{III.4}$$

- The maximum power of each cell is:

$$P_{mp}(cell) = \frac{V_{mp}}{N_s} \tag{III.5}$$

- The series resistance of each cell is:

$$R_s(cell) = \frac{N_p}{N_s} R_s \tag{III.6}$$

- The shunt resistance of each cell is:

$$R_{sh}(cell) = \frac{N_p}{N_s R_{sh}} \tag{III.7}$$

III.6.1 Two-diode model

The figure (III.6) represents the equivalent circuit of a solar cell, made by the parallel connection of two diodes with saturation currents I_{s1} and I_{s2} and diode factors n_1 and n_2, a current source producing the short-circuit current of the cell which depends on the solar illumination. The series resistance Rs takes into account the resistivity of the material and the semiconductor-metal contact. It's value can be determined by the inverse of the slope of the I(V) characteristic for the open circuit voltage V_{co}. The parallel resistance R_{sh} reflects the presence of a leakage current in the junction.[13, 34]

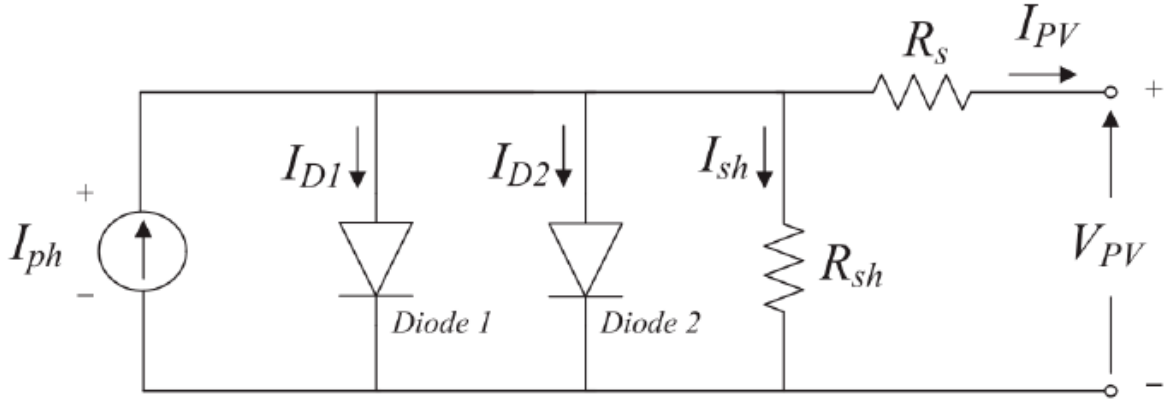

Figure III.6: Equivalent diagram of the two-exponential model.

The characteristic equation is deduced in a direct way from Kirchhoff's law.

$$I_{pv} = I_{ph} - I_{d1} I_{d2} - I_{sh} \tag{III.8}$$

- I_{ph} : photonic current.
- I_{d1} : diode current 1.
- I_{d2} : diode current 2.

Since the diode is a non-linear element, it's I-V characteristic is given by the relation.

$$I_{d2} = I_{s1}(e^{\frac{V_d}{n_1 V_t}} - 1) \tag{III.9}$$

$$I_{d2} = I_{s2}(e^{\frac{V_d}{n_2 V_t}} - 1) \tag{III.10}$$

$$I_{sh} = \frac{V_{pv} + Ipv.R_s}{R_{sh}} \tag{III.11}$$

with :

- $V_t = KT_c/q$: representing the thermodynamic potential.
- T_c: is the absolute temperature.
- q: electron charge constant, $(1.602.10^{-19}C)$.
- K: Boltzmann constant $1.38.10^{-23}$ j/k.
- I_{sh}: Current flows through the shunt resistor.

The electric current produced by the cell is then given by the following expression :

$$I_{pv} = I_{ph} - I_{s1}(e^{\frac{V_{pv}+I_{pv}.R_s}{V_t.n_1}} - 1) - I_{s2}(e^{\frac{V_{pv}+I_{pv}.R_s}{V_t.n_2}} - 1) - \frac{V_{pv}+I_{pv}.R_s}{R_{sh}} \tag{III.12}$$

The photon current related to the illumination, to the temperature and to the photon current measured at the reference conditions is given by :

$$I_{ph} = I_{ph0}\frac{E}{E_0}[1 + (T - T_0)(5.10^{-4})] \tag{III.13}$$

with :

- E: illumination $(E_0 = 1000W/m^2)$.
- T: temperature in °K (T_0 =298 K).
- I_{ph0}: photo-current generated by the diode at T_0=298K. (25°C).

Diode saturation currents :

$$I_{s1} = K_2 T^3 e^{-\frac{E_g q}{n_1 TK}} \tag{III.14}$$

$$I_{s2} = K_2 T^{\frac{3}{2}} e^{-\frac{E_g q}{n_2 TK}} \tag{III.15}$$

with :

- E_g = Gap energy of the semiconductor.
- $K_1 = 1.2A/cm_2.K_3$.
- $K_2 = 2.9A/cm_2.K_5/2$

III.6.2 One-diode model

The operation of a photovoltaic module is described by the "standard" one-diode model established by Shocky for a single PV cell. It is generalized to a PV module by considering it as a set of identical cells connected in series or in parallel. A simpler description is obtained from the one-exponential model. This model has one less diode compared to the two-exponential model, which implies that this model has one less exponential in the current-voltage characteristic equation.

A photovoltaic cell can be described in a simple way as an ideal current source which produces a current I_{ph} (equation (III.13) proportional to the incident light power, in parallel with a diode which corresponds to the P-N transition area It is also known as L3P (Lumped, 1 Mechanism model with 3 Parameters.The equivalent electric diagram of the PV cell for this model is represented by the figure (III.7).[13, 34]

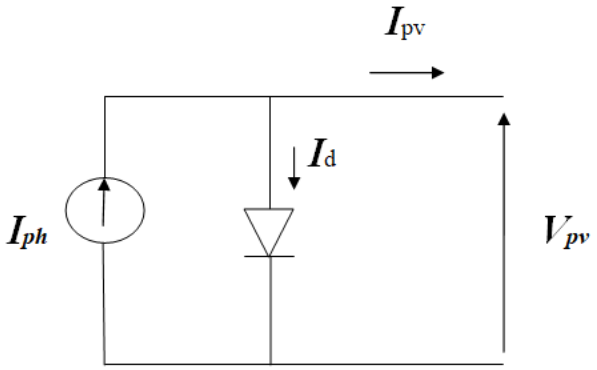

Figure III.7: Equivalent diagram of the model with an L3P exponential

In the case of monocrystalline silicon solar cells, the hypothesis of an ideal cell is considered. The ideality factor is then considered equal to unity.

The characteristic equation is deduced in a direct way from Kirchhoff's law:

$$I_{pv} = I_{ph} - I_d \tag{III.16}$$

The diode being a nonlinear element, its I-V characteristic is given by the relation (III.17)

$$I_d = I_s(e^{\frac{V_d}{V_t}} - 1) \tag{III.17}$$

The current drawn is equivalent to :

$$I_{pv} = I_{ph} - I_s(e^{\frac{V_d}{V_t}} - 1) \tag{III.18}$$

The diode saturation current is assumed to vary with temperature according to the expression (IV.19):

$$I_s = I_{s_ref}(\frac{T_c}{T_{cref}})^3 e^{\frac{q.E_{gap}}{n.K}\frac{1}{T_{cref}} - \frac{1}{T_c}} \tag{III.19}$$

III.7 Converters

The DC-DC converter plays a crucial role in optimizing the power output of the PVG (presumably referring to a photovoltaic system) by employing the MPPT extraction algorithm. This algorithm determines the ideal voltage for the PVG to achieve maximum power. Consequently, a duty cycle D is calculated to regulate the DC-DC converter.

When it comes to electronic devices in new technologies, they need to fulfill specific criteria such as high quality, reliability, compact size, lightweight, and affordability. Linear power regulators, which utilize current or voltage dividers, can deliver a high-quality output voltage.

On the other hand, switching controllers known as DC-DC converters employ semiconductor-based electronic switches like thyristors, power transistors, or IGBT due to their low power loss during switching.These converters offer high energy conversion efficiency and can operate at high frequencies. Increasing the operating frequencies enhances the dynamic properties of DC-DC converters, enabling them to respond quickly to rapid changes in the load current or input voltage.[13, 32]

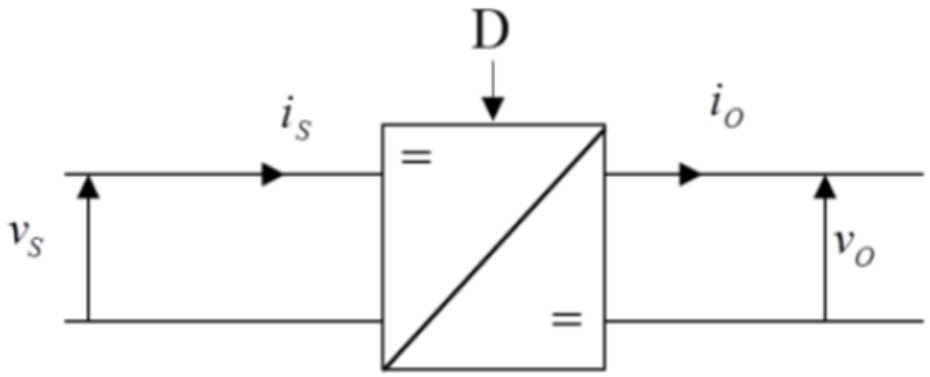

Figure III.8: Symbol of a DC-DC chopper.[13]

Figure (III.8) shows the DC-DC converter that links the DC voltage source to the load. It is considered as a transformer with continuous electrical quantities. The performance of the DC-DC converter allows it to regulate the DC output voltage.

well as load and line variations and reduce DC output voltage harmonics below the tolerated level. There are several types of DC-DC choppers on the market, in this chapter we will review the following converters:

III.7.1 Step-Down Converter (Buck)

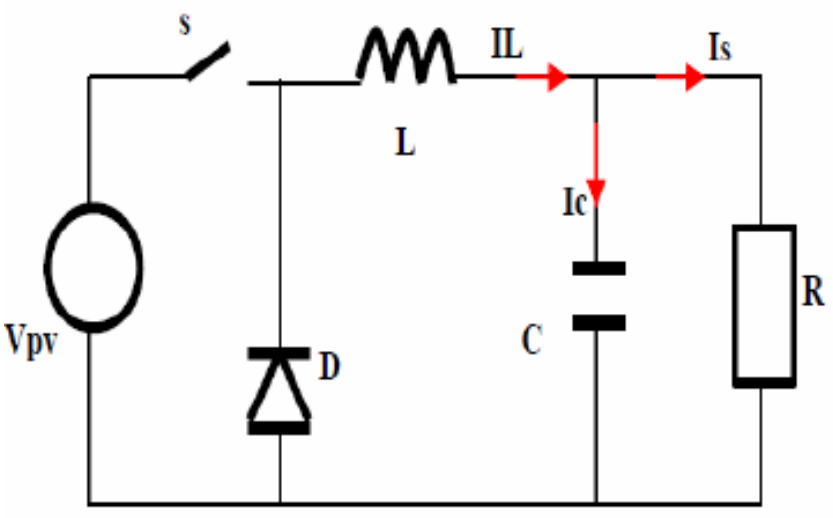

Figure III.9: Electric circuit of the step-down chopper

The key components of a buck chopper are the inductor (L), diode (D), capacitor (C), and switch (s).

The capacitor is charged by the switch (S) which maintains the voltage across its terminals until the opening of (S) which discharges its energy through the diode on the load for a period of

operation (T).

Operating cycle

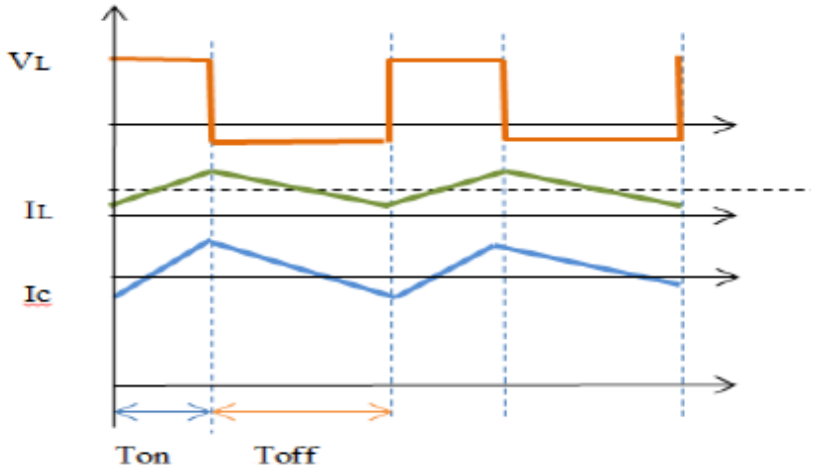

Figure III.10: Characteristic of the voltage and currents in the transistor and the inductance of a Buck converter

The mathematical equation characterizing the inductance current is:

$$\frac{dIL}{dt} = \frac{V_{pv} - U_{dc}}{L} \tag{III.20}$$

The voltage at the load terminal is:

$$V_{pv} = V_{dc} + V_L \tag{III.21}$$

with :

$$\frac{T_{on}}{T} \tag{III.22}$$

During T_{on} , the switch (S) is in the saturation state, then the inductor (L) is charging and the current in (I_L) is increasing. During T_{off} , the inductor releases the energy to the load and the current (I_L) deprived. The mathematical equation characterizing the inductance current is:

$$\frac{dI_L}{dt} = \frac{-Ud_c}{L} \tag{III.23}$$

The voltage at the load terminal is:

$$V_L = -Ud_c \tag{III.24}$$

III.7.2 elevator chopper (Boost)

The booster chopper is used firstly to adopt the voltage level and secondly to operate the photovoltaic generator at the point of maximum power the block diagram of the booster chopper is presented in figure (III.11):

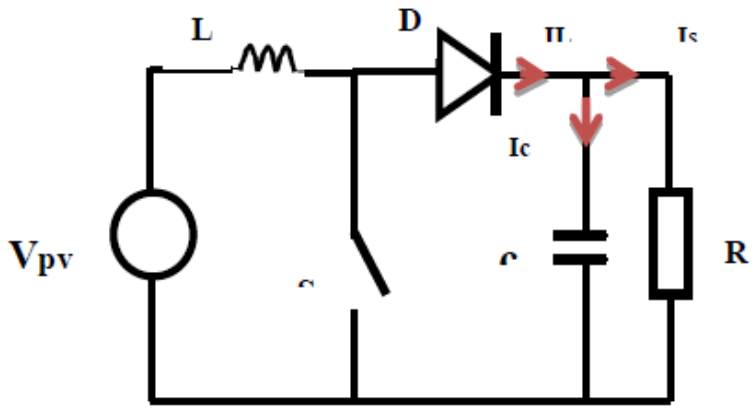

Figure III.11: Model of the booster chopper.

Operating cycle

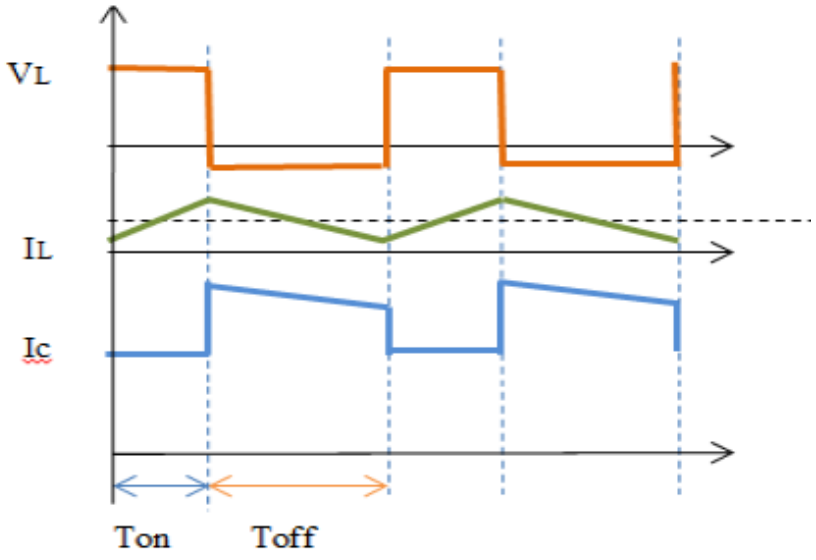

Figure III.12: Model of the booster chopper.

During T_{on} the switch (S) is closed, the inductance stores energy while the current (I_L) is increased.

$$\frac{dI_L}{dt} = \frac{V_{pv}}{L} \tag{III.25}$$

During T_{off}, the switch opens and the inductor (L) generates a voltage which is added to the source voltage which is applied to the load through the diode (D).

$$Ud_c = V_{pv} + V_L \tag{III.26}$$

$$\frac{dI_L}{dt} = \frac{V_{pv} - Ud_c}{L} \tag{III.27}$$

III.7.3 The Buck-Boost Converter

A Buck-Boost converter is a switching power supply which converts a DC voltage into another DC voltage of lower or higher value but of reverse polarity.

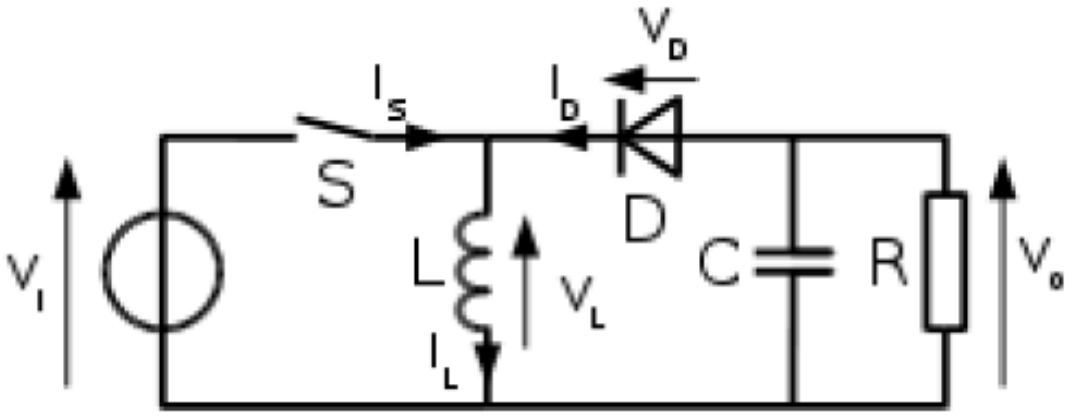

Figure III.13: Diagram of the electrical circuit of a Buck-Boost converter.

During the "on" state, the energy supplied by the source (PV generator) is stored in the inductance L (figure III.13). The energy stored in the inductor L is then delivered to the load during the "off" state.

Due to the presence of diode D, current flows through inductor L only in one direction during both states. Therefore V_{load} has opposite polarity to V_{pv}. For this reason, this circuit is also called an inverting converter. The equations describing this circuit can be obtained in the same way as before. As mentioned earlier, capacitor C_1 backs up the supply voltage V_{pv}, C_2 smooths out the load voltage. In conclusion, the amplitude of V_{load} can be lower or higher than V_{pv} depending on the value of ton and toff :

$$V_{load} = \frac{t_{on}}{t_{off}} V_{pv} = \frac{D}{1-D} V_{pv} \quad \text{(III.28)}$$

III.8 Maximum Power Point Tracking (MPPT)

To achieve the optimum value of the PVG, the tuning stage must be equipped with an MPPT control that operates in its duty cycle based on changes in weather conditions or potential load variations. In this regard, we will incorporate the maximum energy point search orders along with various types of maximum energy into this process.

III.9 Principle

To enable the photovoltaic system to operate at its maximum power points according to their characteristics, specific control laws have been developed to fulfill this requirement. This control technique is referred to as "Search for the Maximum Power Point" or "Maximum Power Point Tracking" (MPPT) in the literature. The fundamental principle of these control methods is to continuously search for the maximum power point (PPM) while ensuring a proper match between the generator and its load, facilitating the efficient transfer of maximum power. Figure (III.14) depicts a basic photovoltaic conversion chain integrated with an MPPT control. The MPPT control is linked to a static converter, which enables adaptation between the PVG and the load, ensuring that the generated power corresponds to its maximum value and is directly transferred to the load.

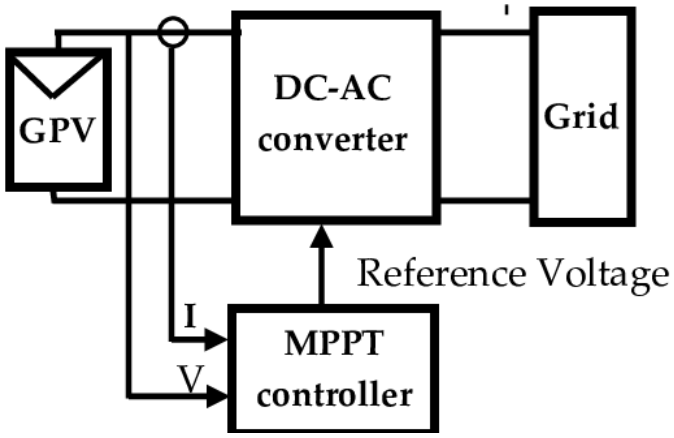

Figure III.14: Photovoltaic conversion chain with static converter controlled by MPPT.[14]

The control technique, therefore, involves automatically adjusting the duty cycle to bring the operating point of the generator to its optimal value, regardless of weather instabilities or sudden variations in the load.

III.10 Classification Of MPPT Commands

MPPT commands can be broadly categorized based on their electronic implementation: analog, digital, or mixed. However, a more intriguing approach is to classify them based on the type of research they conduct and the input parameters utilized by the MPPT command.

III.10.1 Classification of MPPT commands according to input parameters

MPPT commands working from input parameters

There are various MPPT commands that aim to search for the MPP based on the power output evolution of the PVG. For instance, the Perturb and Observe method, conductance increment algorithms, and commands based on proportional relationships between the optimal parameters (V_{opt} and I_{opt}) characterizing the MPP, and the characteristic parameters of the PV module (V_{co} and I_{cc}). Additionally, there are MPPT inspired by neural networks. In these commands, either large computer systems with extensive memory are used, storing all possible cases, or approximate methods are employed. All of these commands offer the advantages of precision and quick response times.

MPPT commands working from output parameters

In the literature, there are also algorithms that rely on the CS output parameters. For instance, there are MPPT commands based on maximizing the output current, primarily utilized when the load consists of a battery. In all systems employing output parameters, an estimation of P_{max} is made based on the converter's efficiency. In essence, the accuracy of this approximation increases with the improvement of the conversion stage. However, it should be noted that systems with a single sensor are generally prone to inherent inaccuracies. Many of these systems were initially designed for space applications.

III.10.2 Classification of MPPT commands according to the type of research

MPPT indirect

These types of MPPT commands utilize the inherent relationship between the measured variables (or) that can be easily determined and the approximate position of the MPP. They also include commands that rely on an estimation of the PVG operating point based on a predefined parametric model. Additionally, there are commands that extend the optimal voltage range by

solely considering variations in cell temperature provided by a sensor. These commands are advantageous due to their simplicity. However, they are primarily designed for low-cost, low-precision systems operating in geographical regions where climate variations are minimal.

MPPT Direct

This type of MPPT control determines the optimal operating point (MPP) based on the currents, voltages, or powers measured within the system. As a result, it can effectively respond to unpredictable changes in the operation of the PVG. Generally, these procedures rely on a search algorithm that determines the maximum point of the power curve without interrupting the operation. To achieve this, the voltage of the operating point is incrementally adjusted at regular intervals. If the output power is higher, the search direction is maintained for the next step; otherwise, it is reversed. This leads to the actual operating point oscillating around the MPP. This fundamental principle can be preserved by employing other algorithms to mitigate misinterpretations. Errors can arise, for example, from incorrect search direction caused by a sudden increase in radiation levels leading to a power increase. The determination of the PV generator's power value, essential for MPP tracking, requires the measurement of generator voltage and current, followed by multiplying these two variables. Other algorithms introduce sinusoidal variations as small signals in the converter's switching frequency to compare the alternating component with the direct component of the PVG's voltage. This helps position the PVG's operating point as close as possible to the MPP. The advantage of these types of commands lies in their precision and rapid response.

III.11 MPPT algorithms

The maximum power can be attained by utilizing a DC/DC converter placed between the GPV and the load, with the duty cycle adjusted to achieve impedance matching. The crucial question then arises: how should this duty cycle be varied and in which direction to achieve maximum power? Automatic tracking can be accomplished using various algorithms, which serve as the core of the MPPT controller. These algorithms are implemented in a microcontroller or personal computer to facilitate maximum power tracking. The algorithm modifies the duty cycle of the DC/DC converter to optimize the output power of the module and operate it at its maximum power point. Numerous MPPT algorithms can be found in the literature, and among these algorithms.

- Disturbance and Observe Algorithm (P and O, Disturbance and Observe) Fuzzy Logic Based Algorithm.
- MPPT Algorithm A Base of artificial neural networks.
- Algorithm based on the measurement of a fraction of the current.

- Algorithm Based on the Measurement of a Fraction of Voltage.

III.12 Perturbation and Observation (P & O) Algorithm

The 'P & O' perturbation and observation method is widely used in the industrial environment due to its easy implementation algorithm. This method operates by perturbing the system through increasing or decreasing the operating voltage of the module and observing its impact on the array's output power. In Figure (III.15), it can be observed that when the operating voltage is perturbed in a specific direction and the power increases ($\frac{d_p}{d_v} > 0$), it indicates that the perturbation has moved the operating point closer to the MPP. The P&O algorithm will then continue perturbing the voltage in the same direction. Conversely, if the power decreases ($\frac{d_p}{d_v} < 0$), it signifies that the perturbation has moved the operating point away from the MPP. In such cases, the algorithm will reverse the direction of the next perturbation.

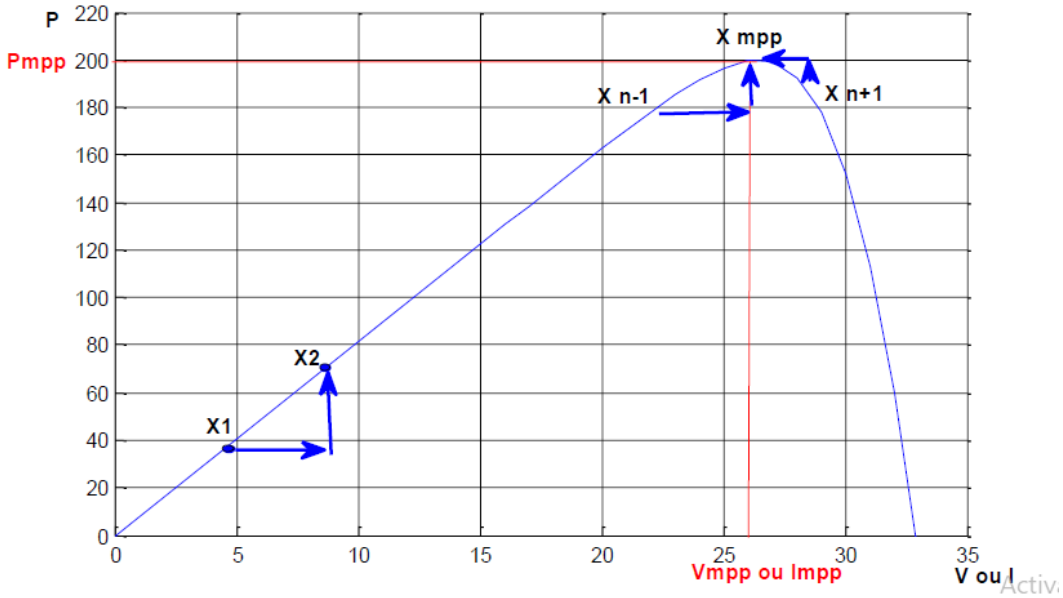

Figure III.15: Photovoltaic conversion chain with static converter controlled by MPPT.[15]

case n	ΔV	ΔP	$\frac{\Delta P}{\Delta V}$	follow direction	control action
1	+	+	+	Good	increment $V_{ref} = V_{ref} = \Delta V$
2	-	-	+	Bad	increment $V_{ref} = V_{ref} = \Delta V$
3	+	-	-	Bad	decrement $V_{ref} = V_{ref} = \Delta V$
4	-	+	-	Good	decrement $V_{ref} = V_{ref} = \Delta V$

Table III.1: Principle of the P&O algorithm

The P&O algorithm (Figure III.15) offers the advantages of precision and speed of reaction. It enables the determination of the maximum power point (PPM) under varying sunlight conditions, temperature, or degradation levels. However, this algorithm has a few drawbacks:

- Oscillations around the PPM during normal operating conditions.
- Poor convergence of the algorithm in cases of sudden temperature and/or sunlight variations.
- It should be noted that these oscillations can be reduced by using smaller incremental steps, but this comes at the expense of longer convergence time. Therefore, a trade-off must be made between accuracy and speed when selecting the update step size.

Figure (III.15) illustrates the flowchart of the algorithm for the "P&O" method, as it should be implemented in the control microprocessor. Based on Figure (III.15), the voltage (V) and current (I) are measured to calculate the current output power (P_k) of the array. This calculated power value (P_k) is then compared to the value from the previous measurement ((P_{k-1}). If the output power has increased, the disturbance will continue in the same direction. However, if the power has decreased since the last measurement, the disturbance of the output voltage will be reversed in the opposite direction of the previous cycle.[15]

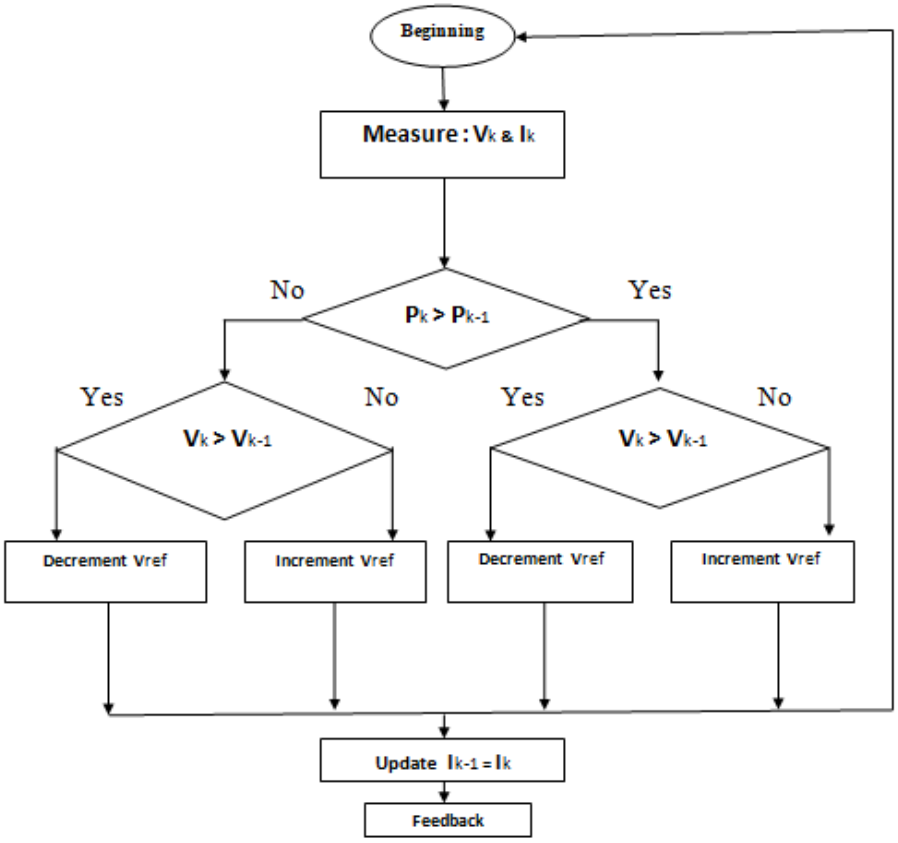

Figure III.16: Perturbation and Observation MPPT Algorithm Flowchart

III.13 Influence of illumination on the I(V) and P(V) curves

The power delivered by a PV generator is dependent on the amount of irradiation it receives, as illustrated in the figures (III.17). In fact, for a given module, the impact of the illumination can be approximated by a current source that is directly proportional to the irradiation. The subsequent graphs depict the characteristics of P(V) and I(V) respectively for a photovoltaic module with a constant temperature (T=25°C) and varying insolation.[35]

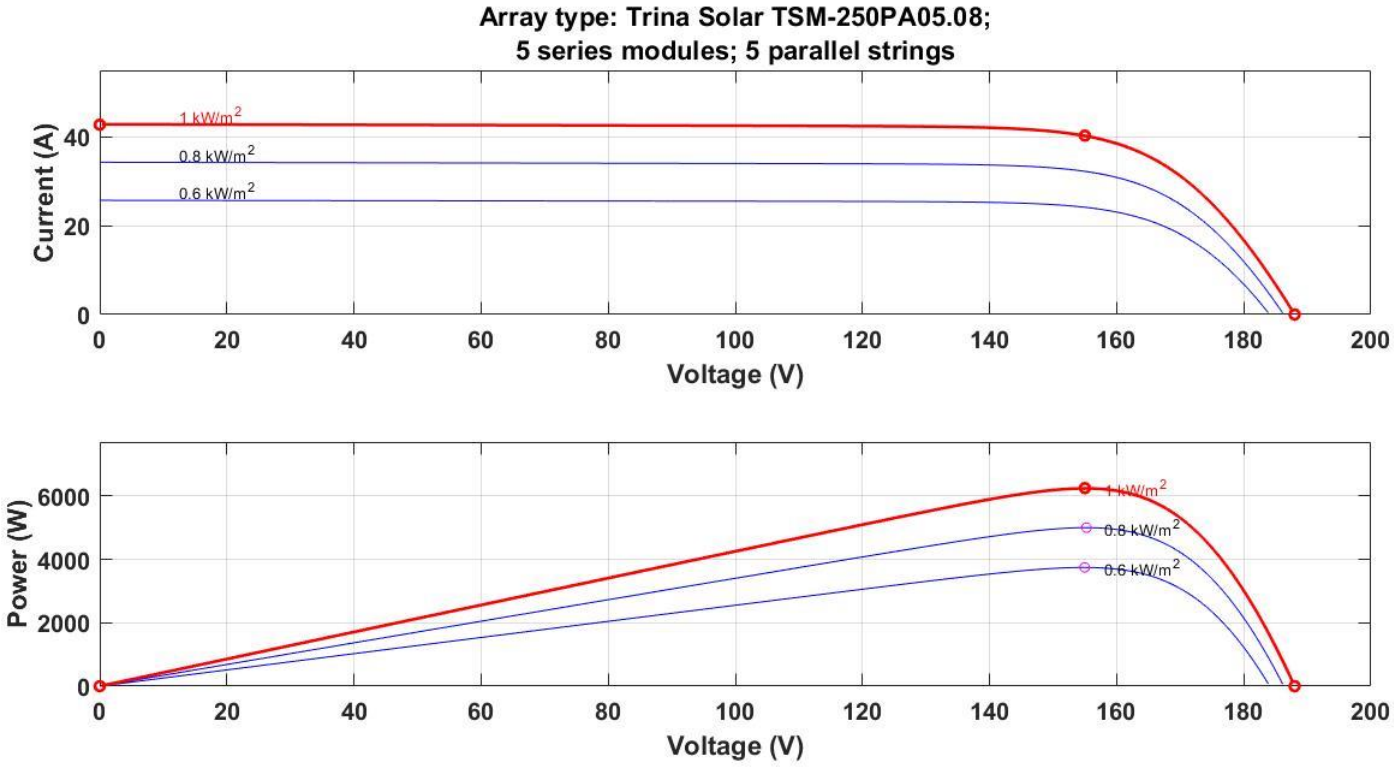

Figure III.17: Simulation results of the I(V) and P(V) characteristics of a PV module according to different irradiations at T=25°C.

We can also observe that the current is directly proportional to the solar radiation. Conversely, the voltage experiences relatively little degradation. Hence, we can conclude that the panel is capable of providing a suitable voltage, even under low light conditions.[35]

III.14 Influence of temperature on I(V), P(V) curves

The graphs represent the I(V) and P(V) characteristics respectively of a photovoltaic module for constant sunshine ($S = 1000W/m^2$) and variable temperature.

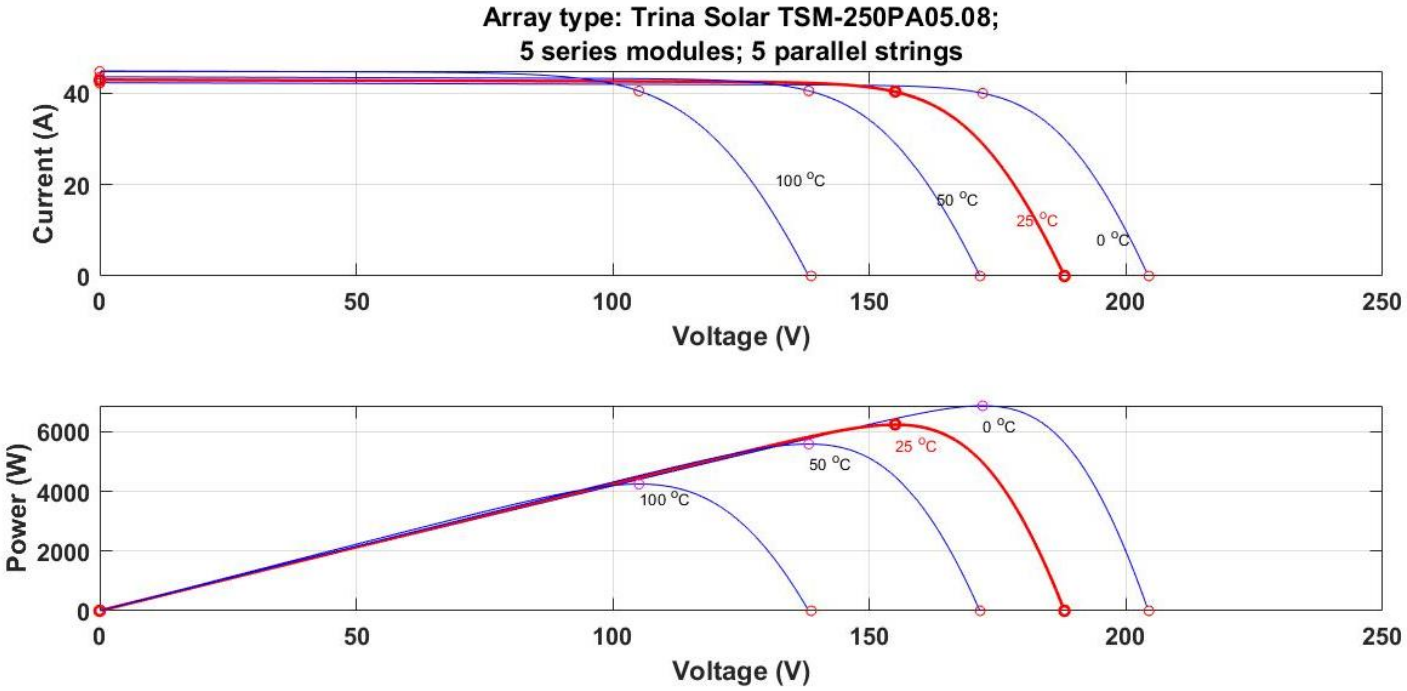

Figure III.18: Simulation results of the I(V) and P(V) characteristics of a PV module according to different temperatures at $S = 1000W/m^2$.

It is evident that the temperature has a minimal impact on the value of the short-circuit current. However, the open circuit voltage experiences a significant decline as the temperature rises, resulting in a decrease in extractable power. When designing an installation, it is crucial to consider the variation in site temperature, as it is directly related to the temperature of the cells.

Furthermore, it is important to note that the module's power decreases by approximately 0.5% for every degree of cell temperature increase above 25°C.[35]

III.15 Simulation of PVG with boost converter

III.15.1 simulation results

The figure (IV.19) represents the voltage, current and power results under a temperature of 25°C and a light intensity of $S = 1000W/m^2$. With 12 panels connected in series and 8 in parallel.

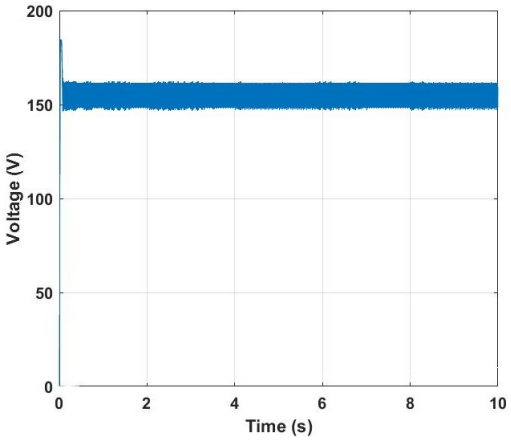

(a) Voltage (PVG)

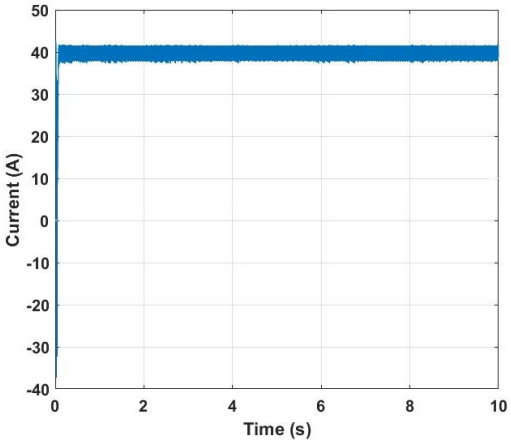

(b) Current (PVG)

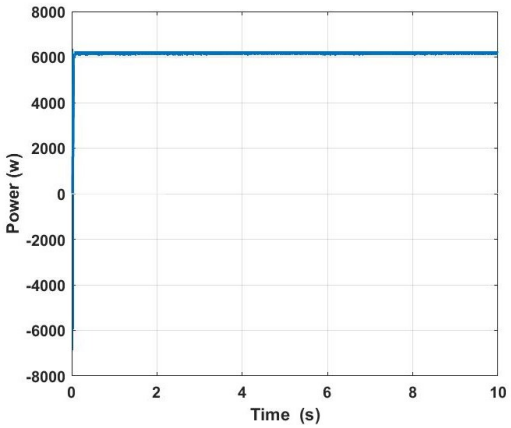

(c) Power(PVG)

Figure III.19: Results of simulation

the figure (III.20) represent voltage (DC) with MPPT regulator and boost converter.

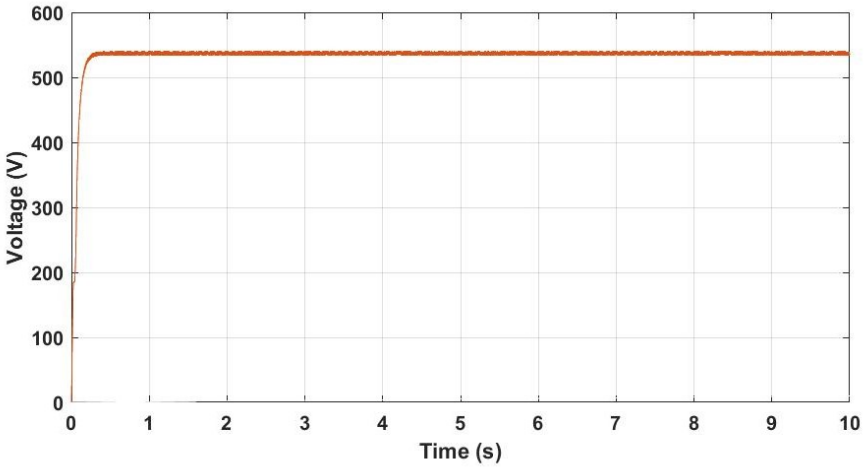

Figure III.20: Voltage (DC)

III.16 Conclusion

In this chapter, we familiarized ourselves with the photovoltaic generator and the natural factors that influence the current and voltage intensity. We also discussed one of the most important methods for addressing the challenges posed by natural variations in energy production, namely Maximum Power Point Tracking (MPPT). We explored several algorithms, including the Perturb and Observe (P&O) algorithm, and provided a simplified explanation of its functioning.

In addition, we examined the characteristics of solar panels and their impact on temperature and light radiation variations. Finally, we presented the simulation results of the photovoltaic generator.

Chapter IV

Neural control by DTC

IV.1 Introduction

Artificial neural networks find applications in a variety of fields, encompassing image processing, classification, process estimation, and electrical system control. Numerous studies have employed artificial neural networks for direct torque control (DTC). The chapter asserts that ongoing research is focused on applying intelligent technologies, like ANN-based DTC, for a more effective management of switch states, instead of relying on a switch table and two hysteresis controllers. In the PMSM direct control system, and we also intend to replace the PID controller with a neural network, aiming to reduce stator flux ripples, torque ripples, and enhance motor rotational speed.[36][37]

IV.2 Artificial Neural Network

An Artificial Neural Network (ANN) is a computational model inspired by the structure and functioning of the human brain's neural networks. It's a type of machine learning algorithm that is capable of learning patterns and relationships from data. ANN consists of interconnected nodes, also known as artificial neurons, which are organized into layers. These layers include an input layer, one or more hidden layers, and an output layer.[36][38]

IV.3 The key components of an ANN

IV.3.1 Neurons (Nodes)

Neurons are the basic building blocks of an ANN. Each neuron receives inputs, performs computations on those inputs, and produces an output. Neurons are organized into layers, with each layer serving a specific purpose.[36][38]

IV.3.2 Layers

An ANN typically consists of three main types of layers:

- Input Layer: Neurons in the input layer receive the initial data or features.
- Hidden Layers: These intermediate layers perform complex computations and transformations on the input data. The number of hidden layers and the number of neurons in each layer can vary depending on the specific problem.
- Output Layer: Neurons in the output layer produce the final results or predictions.

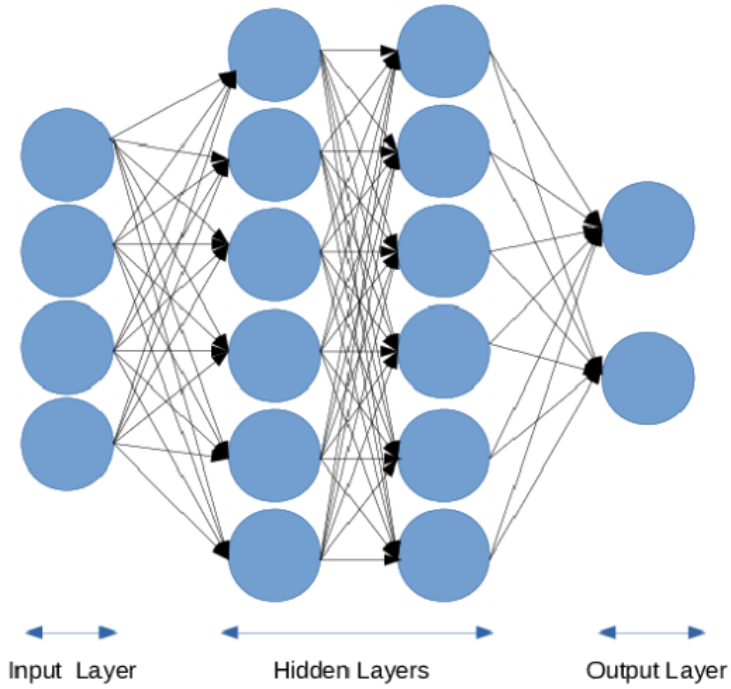

Figure IV.1: layers Diagram

IV.3.3 Connections (Synapses)

Neurons in one layer are connected to neurons in the adjacent layers through weighted connections. These connections carry signals between neurons and determine the strength of influence one neuron has on another.[36][38]

IV.3.4 Weights and Biases

Each connection between neurons has an associated weight, which determines the impact of the input on the neuron's output. Additionally, each neuron has a bias term that can shift its activation function.[36][38]

IV.3.5 Activation Function

Neurons apply an activation function to the weighted sum of their inputs to produce an output. Activation functions introduce non-linearity to the model, allowing it to learn complex relationships in the data.

IV.3.6 Training

Neural networks learn from data through a process called training. This involves presenting the network with a labeled dataset, computing the difference (error or loss) between the predicted

output and the actual target, and then adjusting the weights in the network to minimize this error. The most common optimization algorithm used for this purpose is backpropagation, which calculates the gradient of the loss function with respect to the network's weights and updates them accordingly.

The process of training an ANN involves feeding it a labeled dataset and adjusting the weights and biases of the connections to minimize the difference between predicted outputs and actual outputs. This is typically done using optimization techniques like backpropagation, where the network iteratively updates its parameters to improve its predictions.

ANN are used for a wide range of tasks, including image and speech recognition, natural language processing, classification, regression, and control systems. They have the ability to learn from large amounts of data and can generalize patterns to make predictions on new, unseen data.[36][38]

IV.4 Proposed DTC-ANN

The proposed DTC-ANN consists of two ANN controllers, the first replaces the switch table providing the voltage vector, the inputs to the ANN controller are stator flux error C_{flux}, C_{cpl} error torque and sector number N, depend This ANN is on feed-forward backpropagation with a number of hidden layers containing a group of neurons in each layer respectively and logsig as the activation functions, the output layer contains three neurons that provide the voltage vector, the proposed ANN switching table is shown in Fig(IV.2).[38]

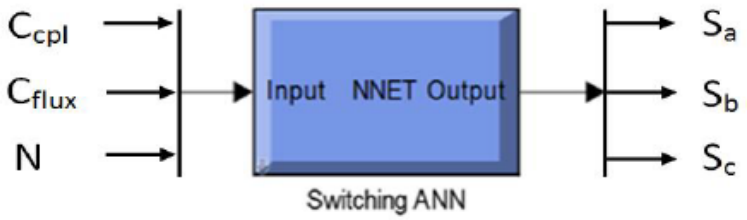

Figure IV.2: The neural networks Switching Table with Matlab /Simulink

The second ANN controller replaces the traditional IP, and it is based on feed-forward back propagation with several hidden layers containing a neuron group in each layer respectively and logsig as activation functions for the first, second layer, etc. but the last layer has a function Purlin activation, controller inputs ANN is the difference between the measured velocity Wm and the reference velocity Wref, but the output layer is Ceref. Figure (IV.3) shows the proposed ANN

speed controller. The weights are determined by the training algorithm.[38]

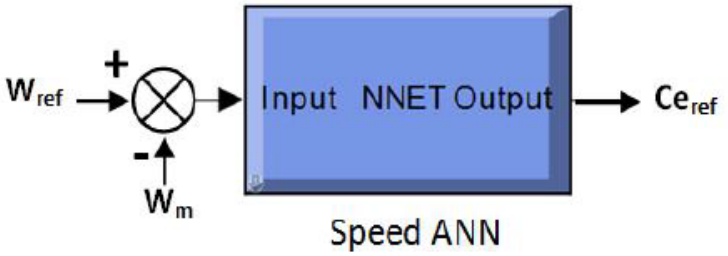

Figure IV.3: The Neural Networks Speed Controller.

The proposed DTC-ANN scheme including both ANN controllers is illustrated in the Fig.(IV.4).

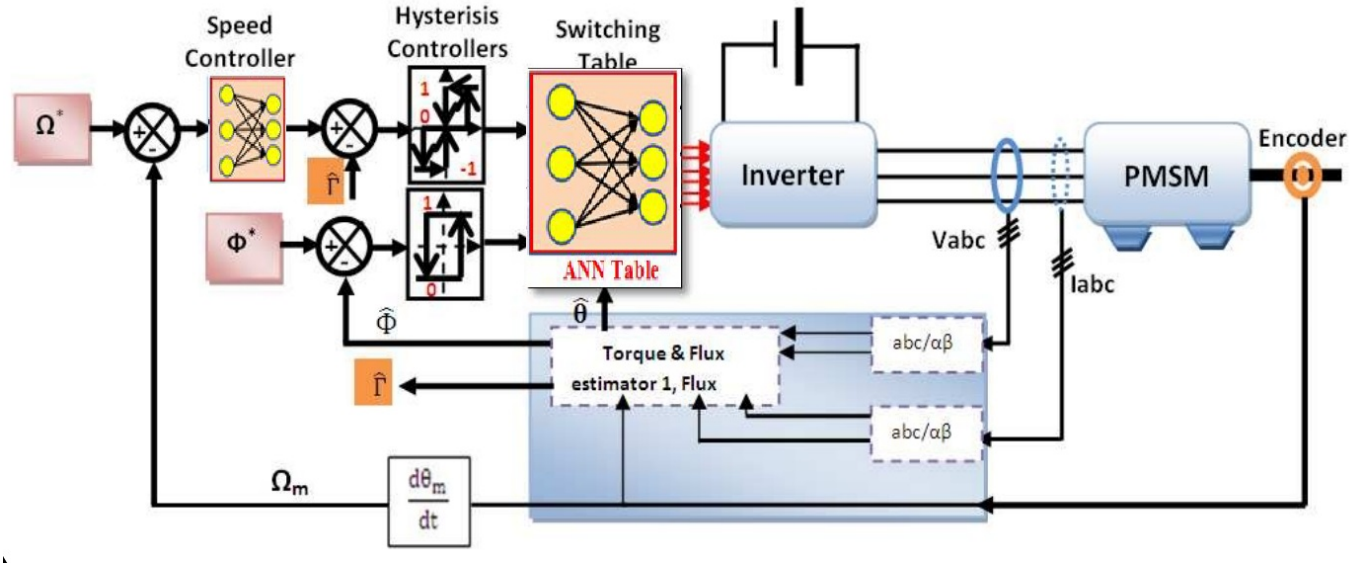

Figure IV.4: DTC-ANN scheme.

IV.5 Simulation results

IV.5.1 Block diagram

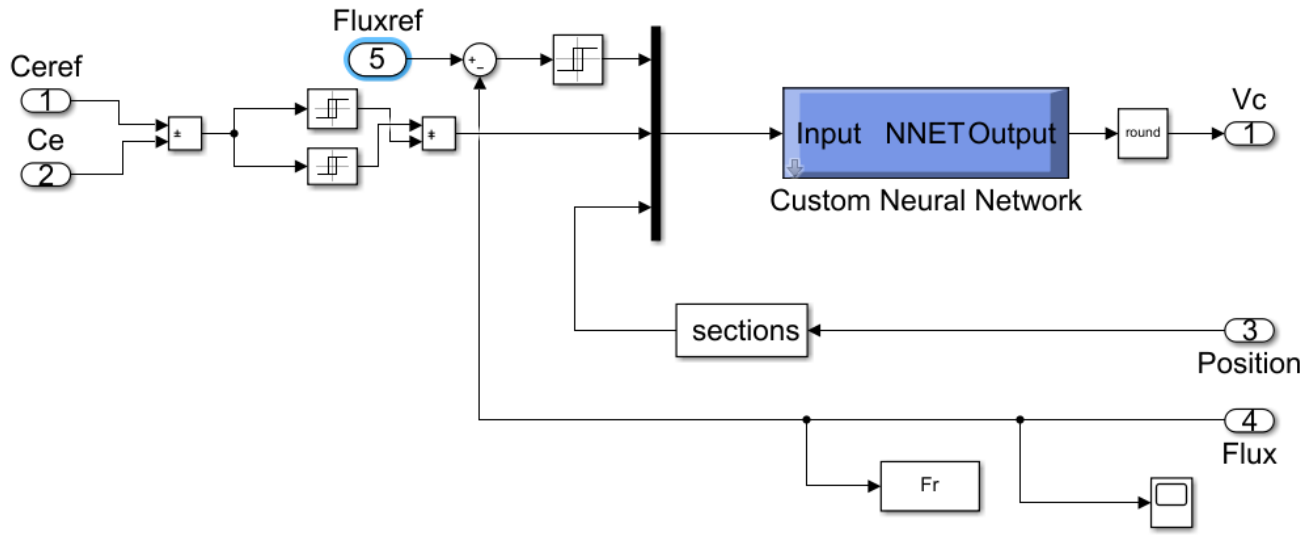

Figure IV.5: Scheme bloc of replaces the switch table with ANN .

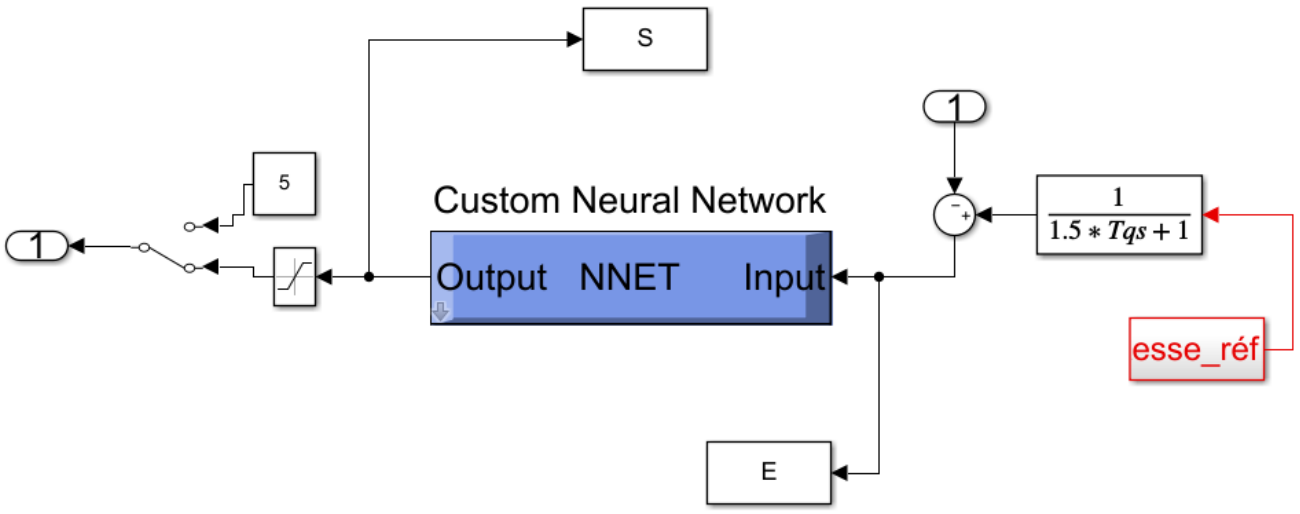

Figure IV.6: Scheme bloc of replaces PID with ANN .

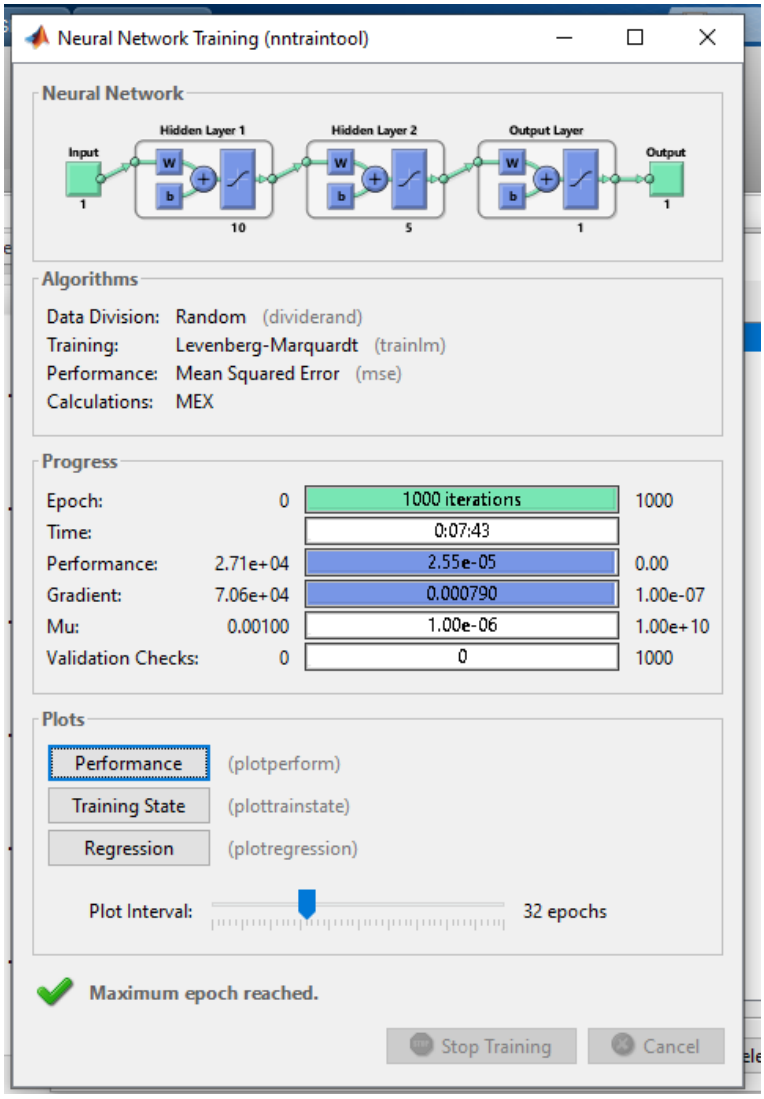

(a) Replaces PID with ANN

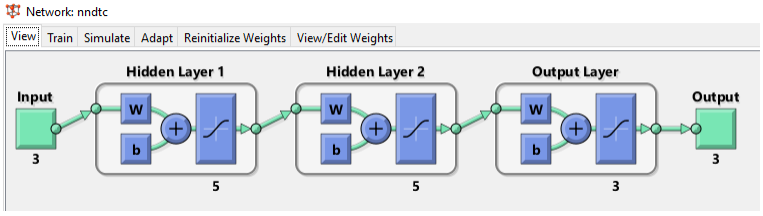

(b) Replaces the switch table with ANN

Figure IV.7: The operation and the evolution of learning

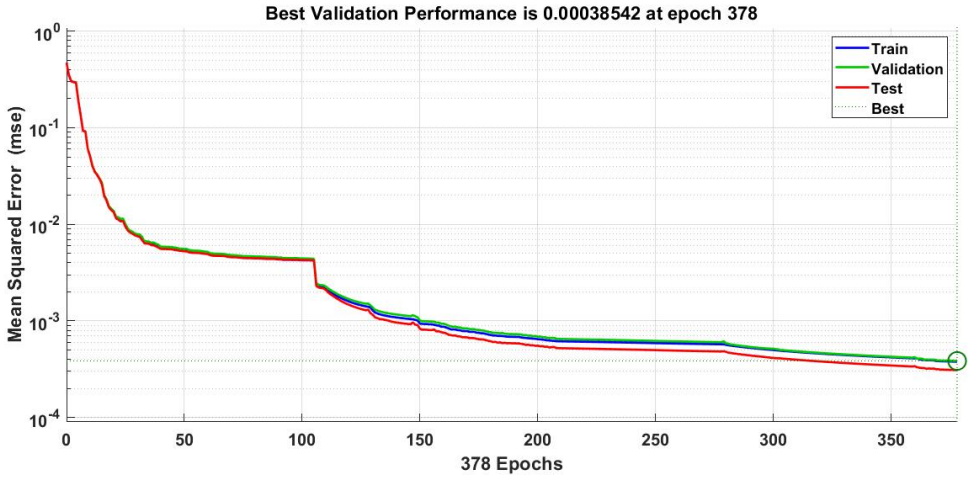

Figure IV.8: Convergence of the RNA output towards its target (Target).

After replacing the switch table with ANN and PID with ANN and connecting the PV generator, we obtained the following results

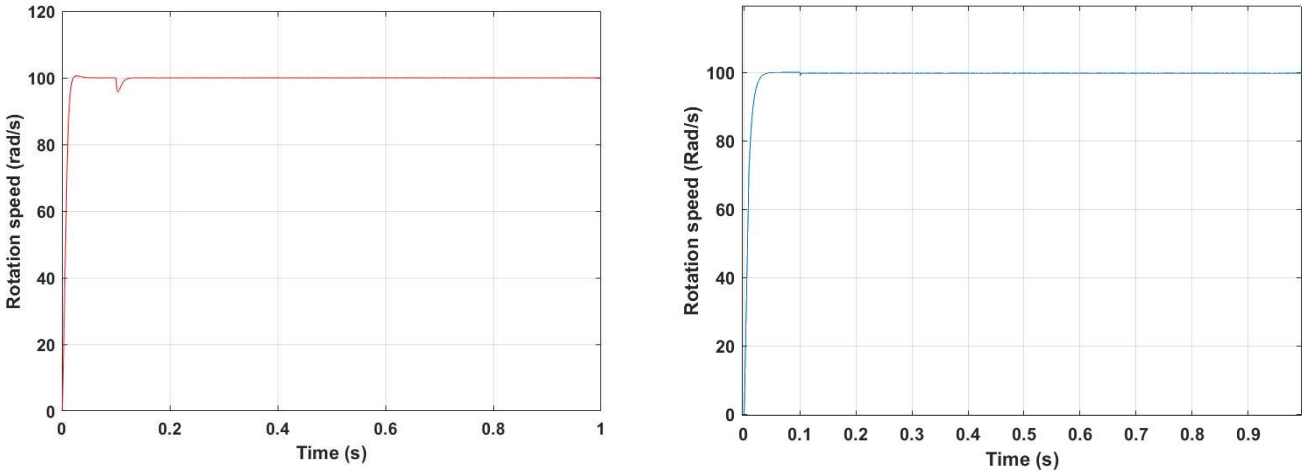

(a) Without ANN

(b) With ANN

Figure IV.9: Rotation speed

The figure (IV.9) shows that with the presence of the neural network, we notice that the speed decrease of 0.1 second disappears due to the applied load.

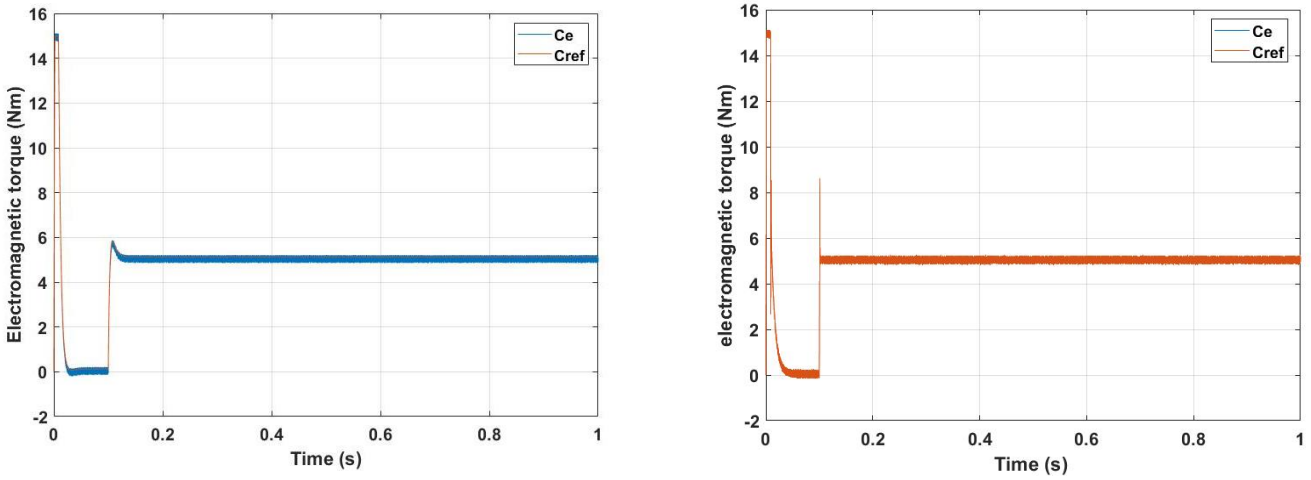

(a) Without ANN (b) With ANN

Figure IV.10: Electromagnetic torque

Likewise, in the figure (IV.10) with the neural network, we notice that the ripple disappears at 0.1 second.

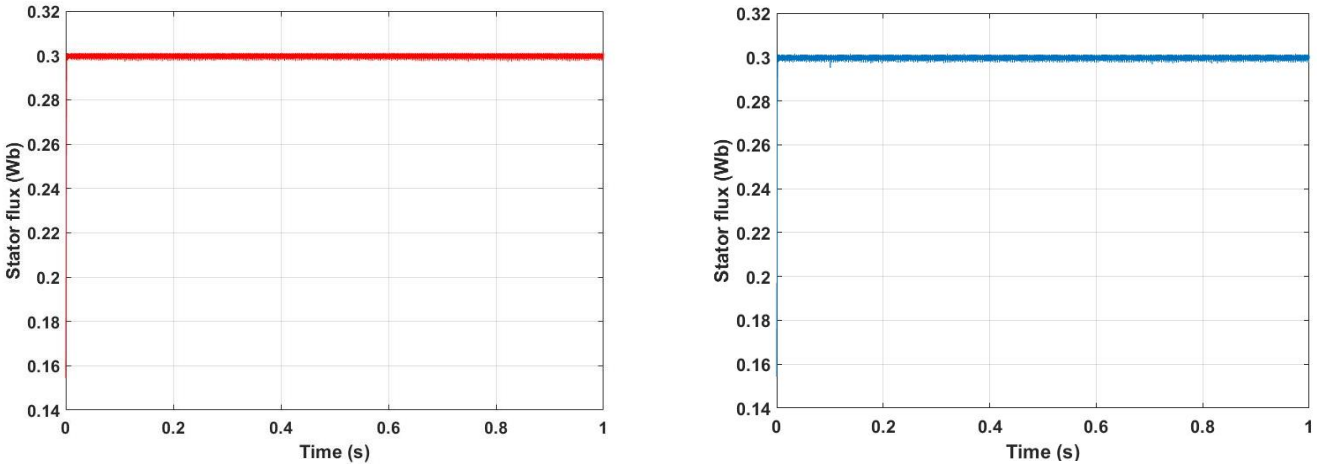

(a) Without ANN (b) With ANN

Figure IV.11: Stator flux

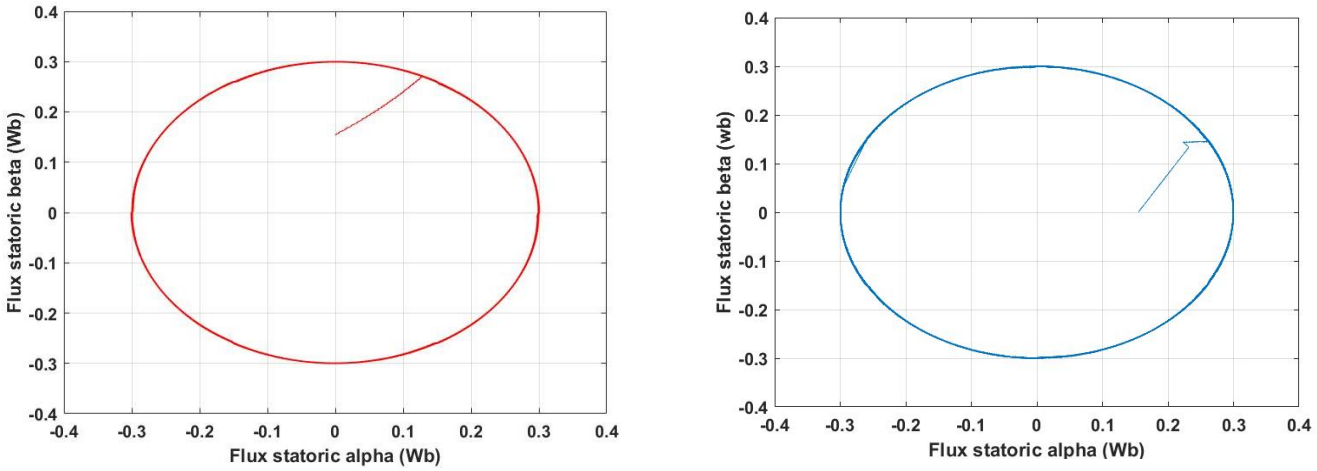

(a) Without ANN

(b) With ANN

Figure IV.12: Flux stator alpha and beta

IV.6 Conclusion

In this chapter, we introduced the fundamental principles of neural networks, which draw inspiration from the human brain. Advancements in neurobiology and the utilization of advanced theoretical tools such as the backpropagation algorithm have led to the development of more intricate models. Integrating artificial neural networks into control systems offers the potential for defining processes, adapting the network, and effectively managing the system. The subsequent exploration focuses on applying this technique as an alternative to hysteresis comparisons.

Towards the end of this chapter, we conducted simulations where we replaced switch table and the PID control unit with a neural network in the direct control system of a permanent magnet motor and we also connecting the PV generator to the motor. The results demonstrated improved speed stability, even in the presence of load changes

General Conclusion

In the first chapter, we covered various aspects related to the permanent magnet synchronous motor. We discussed its essential components, operating methods, and working principle. Additionally, we explored its mathematical model, which involved converting from three phases to two phases in two reference frames. Simulations were performed to analyze the motor's behavior under both unloaded and loaded conditions.

Furthermore, we presented the structure of Direct Torque Control (DTC) as an efficient and straightforward method for driving a Permanent Synchronous Motor (PMSM). This control strategy demonstrated robustness against variations in machine parameters and exhibited commendable performance in terms of torque and flux.

Moving on, we delved into the photovoltaic generator and its interaction with natural factors influencing current and voltage intensity. We emphasized the significance of Maximum Power Point Tracking (MPPT) as a solution to address the challenges posed by natural variations in energy production. The Perturb and Observe (P&O) algorithm was discussed as one of the prominent MPPT algorithms. We also examined the characteristics of solar panels and their impact on temperature and light radiation variations, followed by the presentation of simulation results for the photovoltaic generator.

Lastly, we introduced neural networks, drawing inspiration from the human brain, and highlighted their role in control systems. The backpropagation algorithm and other advanced tools were discussed. The application of neural networks as an alternative to hysteresis comparisons was explored. Simulations were conducted, replacing the PID control unit with a neural network in the direct control system of a permanent magnet motor. The results showcased improved speed stability, even in the presence of load changes.

Perspectives for the development of this work include:

- Further optimization of control algorithms and integration of advanced machine learning techniques.

- Experimental validation and system integration for practical applications.
- Exploration of fault diagnosis, cost optimization, and industrial implementation for commercialization.

Bibliography

[1] N. Bernard, "Machine synchrone: de la boucle ouvertea l'autopilotage," *Revue 3EI*, vol. 30, pp. 24–39, 2002.

[2] F. De La Torre, "21507-19 accionamientos electromecánicos máquina sincrónica," 2019.

[3] S. J Chapman, *Electric machinery fundamentals*. McGraw-hill, 2004.

[4] M. BENOUATAS, F. HAMIDIA, and A. ABBADI, "Amelioration de la commande dtc appliquee a la machine synchrone a aimant permanant par la logique floue type-2," 2018.

[5] R. Ouerdane, *Commande des machine synchrone à aimants permanents à saillance inverse*. PhD thesis, 2017.

[6] H. M. Ilyes, *Commande sans capteur de vitesse d'un moteur synchrone à aimants permanents (MSAP) par l'utilisation de la commande directe du couple et d'un observateur de vitesse à mode glissant*. PhD thesis, 2012.

[7] H. Bensaadi, *Commande DTC-SVM d'une Machine Synchrone à Aimants Permanents*. PhD thesis, Université de Batna 2, 2012.

[8] C. Bousnoubra and M. S. Merzoug, "Commande dtc d'un moteur synchrone à aimants permanents avec estimation de la vitesse en utilisant le filtre de kalman," 2020.

[9] B. Houara, "Commande dtc prédictive de la msap," 2017.

[10] I. KHELIF, *La Commande Direct du Couple D'une Machine Synchrone A Aimants Permanents (MSAP)*. PhD thesis.

[11] K. Chikh, M. Khafallah, and A. Saâd, "Improved dtc algorithms for reducing torque and flux ripples of pmsm based on fuzzy logic and pwm techniques," *MATLAB-A Fundamental Tool for Scientific Computing and Engineering Applications*, vol. 1, pp. 167–194, 2012.

[12] A. Ibnelouad, A. E. Kari, H. Ayad, and M. Mjahed, *A Comprehensive Comparison of Two Behavior MPPT Techniques, the Conventional (Incremental Conductance (INC)) and Intelligent (Fuzzy Logic Controller (FLC)) for Photovoltaic Systems*, pp. 47–84. Singapore: Springer Singapore, 2019.

[13] M. ATIA, *Contribution à la commande MPPT pour les systèmes photovoltaïques*. PhD thesis, Université M'HAMED BOUGARA-BOUMERDES, 2022.

[14] A. Mohamed Said, B. Bossoufi, S. Motahhir, and I. Saady, "Application of fuzzy sliding mode control on a single-stage grid-connected pv system based on the voltage-oriented control strategy," *Results in Engineering*, vol. 17, p. 100822, 12 2022.

[15] A. E. YAHIA HELLALI, T. BOURAHLA, and A. MORSLI, "Contribution à la commande mppt d'un convertisseur dc-dc avec logiciels matlab et proteus pour les applications photovoltaïques.," 2020.

[16] B. S. Guru and H. R. Hiziroglu, *Electric machinery and transformers*, vol. 726. Oxford university press New York, 2001.

[17] S. Said and S. Hamza, *Commande par Logique Floue 2, Application a un Synchrone a aaimants permanents .* PhD thesis, Universite Amar Thelidji-Laghouat, 2015.

[18] M. S. Merzoug, *Etude comparative des performances d'un DTC et d'un FOC d'une machine synchrone à aimants permanents (MSAP)*. PhD thesis, Batna, Université El Hadj Lakhdar. Faculté des sciences de l'ingénieur, 2008.

[19] L. Benalia, *Commande en tension des moteurs à induction double alimentés*. PhD thesis, Université de Batna 2, 2010.

[20] K. Yahia, *Estimation en ligne de l'état et des paramètres du moteur asynchrone triphasé*. PhD thesis, Université Mohamed Khider Biskra, 2005.

[21] H. Nasma, *Commande DTC flou d'un moteur synchrone à aimant permanent*. PhD thesis, UNIVERSITE DE MOHAMED BOUDIAF M'SILA FACULTE DE TECHNOLOGIE, 2016.

[22] A. AMEUR, *Commande sans capteur de vitesse par DTC d'une machine synchrone à aimants permanents dotée d'un observateur d'ordre complet à modes glissants*. PhD thesis, Université de Batna 2, 2003.

[23] S. Dalib, *The simulation of the direct torque control of permanent magnet synchronous motor*. PhD thesis, Universiti Teknologi Malaysia, 2007.

[24] D. Casadei, F. Profumo, G. Serra, and A. Tani, "Foc and dtc: two viable schemes for induction motors torque control," *IEEE transactions on Power Electronics*, vol. 17, no. 5, pp. 779–787, 2002.

[25] H. Mesloub, *Commande DTC Prédictive D'une Machine Synchrone à Aimants Permanents.* PhD thesis, Université Mohamed Khider-Biskra, 2016.

[26] O. Ouledali, A. Meroufel, and P. Wira, "Commande floue directe du couple d'un msap basée sur ml. i vectorielle," in *1er Colloque international sur l'hydrocarbure, énergie et environnement HCEE, Ouargla*, 2014.

[27] , , , and , "Amélioration des performances de la commande directe du couple de la machine asynchrone," 2017.

[28] S. BOUHAFNA, *Commande par DTC d'un moteur asynchrone apport des réseaux de neurones*. PhD thesis, Université de Batna 2, 2013.

[29] K. Akkouchi, *Commande directe du couple (DTC) d'une machine asynchrone*. PhD thesis, Annaba, 2007.

[30] M. Merzoug and F. Naceri, "Comparison of field-oriented control and direct torque control for permanent magnet synchronous motor (pmsm)," *International Journal of Electrical and Computer Engineering*, vol. 2, no. 9, pp. 1797–1802, 2008.

[31] S. Abouda, *Contribution à la commande des systèmes photovoltaiques: application aux systèmes de pompages*. PhD thesis, Reims, 2015.

[32] S. Ouchen, *Contribution a la commande directe de puissance dediee au filtrage actif, associe a une source photovoltaïque*. PhD thesis, Université Mohamed Khider-Biskra, 2017.

[33] S. Sumathi, *Solar PV and wind energy conversion systems : an introduction to theory, modeling with MATLAB/SIMULINK, and the role of soft computing techniques*. PhD thesis, 2015.

[34] N. AMEL and D. AICHA, *Évaluation des performances d'installations photovoltaïques Application de l'éclairage public.* PhD thesis, Universite Amar Thelidji-Laghouat, 2019.

[35] D. r.BIRANE Mouhoub, *Systèmes multi sources à énergies renouvelables*. 2022.

[36] F. Korkmaz, M. F. Cakır, İ. Topaloğlu, and R. Gurbuz, "Artificial neural network based dtc driver for pmsm," *International Journal of Instrumentation and Control Systems (IJICS) Vol*, vol. 3, pp. 1–7, 2013.

[37] B. MOKHTARI, *DTC intélligente appliquée à la commande de la machine asynchrone*. PhD thesis, Université de Batna 2, 2014.

[38] A. Zemmit, S. Messalti, and A. Harrag, "Innovative improved direct torque control of doubly fed induction machine (dfim) using artificial neural network (ann-dtc)," *International Journal of Applied Engineering Research*, vol. 11, no. 16, pp. 9099–9105, 2016.